Journal of Environmental Management 373 (2025) 123627

Contents lists available at ScienceDirect

Journal of Environmental Management

journal homepage: www.elsevier.com/locate/jenvman

Research article

Sub-daily variability of carbon dioxide, methane, and nitrous oxide emissions from two urban ponds in Brussels (Belgium)

Thomas Bauduin[a,b,*], Nathalie Gypens[a], Alberto V. Borges[b,**]

[a] Ecology of Aquatic Systems, Université Libre de Bruxelles, Brussels, Belgium
[b] Chemical Oceanography Unit, University of Liège, Liège, Belgium

ARTICLE INFO

Handling Editor: Jason Michael Evans

Keywords:
Carbon dioxide
Methane
Nitrous oxide
$\delta^{13}C$-CH_4
Brussels
Urban ponds
Urban ecology

ABSTRACT

Sub-daily variations might significantly impact the estimates of GHG emissions from lakes and ponds. The objectives of this study are (i) to quantify sub-daily variations of the emissions of CO_2, CH_4, and N_2O from two urban ponds (Silex and Pêcheries) in the city of Brussels, (ii) to quantify if the sub-daily variations of GHG emissions were significant compared to their seasonal variations and to inter-pond variations among 20 other ponds in the city of Brussels. The partial pressure of CO_2 (pCO_2), CH_4 concentration, and N_2O saturation level (%N_2O) were measured hourly from dawn to dusk in the Pêcheries turbid-water pond and in the Silex clear-water pond during the four seasons in 2023–2024. pCO_2 followed the day-night cycle of photosynthesis in spring and summer but was more erratic in winter and fall. The variations of CH_4 concentration and %N_2O were on most occasions erratic and difficult to attribute systematically to specific biogeochemical processes. The sub-daily variations of computed GHG emissions were mostly driven by variability in wind speed that usually peaked around mid-day. The comparison with previously acquired seasonal and inter-pond data (n = 22) showed that sub-daily variations of GHG fluxes were lower than seasonal variations, which were in turn lower than inter-pond variations. Consequently, to design sampling strategies to reduce the uncertainty on the estimate of CO_2, CH_4, and N_2O emissions a priority should be given to describe inter-system variability, followed by seasonal variability, and lastly sub-daily variability, in the context of the environmental management of inland waters, including urban ponds.

1. Introduction

Emissions to the atmosphere from inland waters (rivers, lakes, and reservoirs) of greenhouse gases (GHGs) such as carbon dioxide (CO_2), methane (CH_4), and nitrous oxide (N_2O) are quantitatively important for global budgets (Lauerwald et al., 2023). The contribution of CO_2 and CH_4 emissions from small water bodies (ponds) could be disproportionately high compared to larger lakes owing to higher values of areal emission density (Holgerson and Raymond, 2016). Yet, GHG emissions from lakes and ponds remain poorly constrained, due to the paucity of data coverage that is inadequate to correctly capture the enormous spatial heterogeneity and temporal variability (Deemer and Holgerson, 2021; Borges et al., 2022; Ray et al., 2023). This might be even more critical for small water bodies such as ponds that are more abundant (numerous) and potentially more diverse than larger lentic water bodies (Verpoorter et al., 2014; Cael et al., 2017). Emissions of CO_2 and CH_4 span over very wide ranges of values across different lakes and ponds depending on a combination of lake and pond morphology (depth and surface area), catchment topography (slope), climate, and land cover on the catchment (Staehr et al., 2012; Maberly et al., 2013; Casas-Ruiz et al., 2021a, 2021b; Borges et al., 2022). Combined, these factors determine the amount and fate of allochthonous organic carbon inputs to lakes and ponds as well as the level of autochthonous organic carbon production. Both largely determine the production and emission of CO_2 and CH_4 from lakes and ponds to the atmosphere (Staehr et al., 2012; Maberly et al., 2013; Borges et al., 2022). Additional processes such as lateral inputs from CO_2 and CH_4 from ground-water or soil-water will also depend on a combination of the same drivers (Weyhenmeyer et al., 2015).

Additionally, the exchanges of CO_2 and CH_4 in lakes and ponds with the atmosphere also vary across temporal scales from sub-daily to seasonal and to inter-annual. While seasonal (e.g. Borges et al., 2023; Ray

* Corresponding author. Ecology of Aquatic Systems, Université Libre de Bruxelles, Brussels, Belgium.
** Corresponding author.
E-mail addresses: thomas.bauduin@ulb.be (T. Bauduin), alberto.borges@uliege.be (A.V. Borges).

https://doi.org/10.1016/j.jenvman.2024.123627
Received 8 July 2024; Received in revised form 8 November 2024; Accepted 2 December 2024

and Holgerson, 2023) and even decadal (e.g. Xiao et al., 2024) variations of CO_2 and CH_4 emissions have been frequently described, their diel variations are not well documented in lakes and ponds. Yet, diel variations of CO_2 and CH_4 emissions are potentially important and could lead to a substantial revision of estimates since most data are usually acquired during day-time only, and day-time CO_2 and CH_4 emissions are not necessarily equivalent to those during night-time (Sieczko et al., 2020; Rudberg et al., 2021; Golub et al., 2023). Nevertheless, no studies have so far compared consistently and quantitatively the variability of GHG emissions from lakes and ponds at diel scale with variability at larger temporal scales (seasonal) or with the variability across different lakes and ponds driven by differences in productivity, depth, and surface area (Holgerson and Raymond, 2016; DelSontro et al., 2018; Deemer and Holgerson, 2021; Casas-Ruiz et al., 2021a; Borges et al., 2022).

Diel variations of GHG emissions to the atmosphere from inland waters can result from night-day variations of dissolved concentration of the GHGs and/or from the night-day variations of the gas transfer velocity (k). To investigate the diel variations of GHG emissions to the atmosphere from inland waters it is possible to directly measure the GHG fluxes with either eddy-covariance or floating chambers (Podgrajsek et al., 2014; Erkkilä et al., 2018) or to measure the dissolved GHG concentrations and compute the fluxes with modelled k values, usually from parameterizations as function of wind speed (e.g. Klaus and Vachon, 2020; MacIntyre et al., 2021a,b). Each of these three

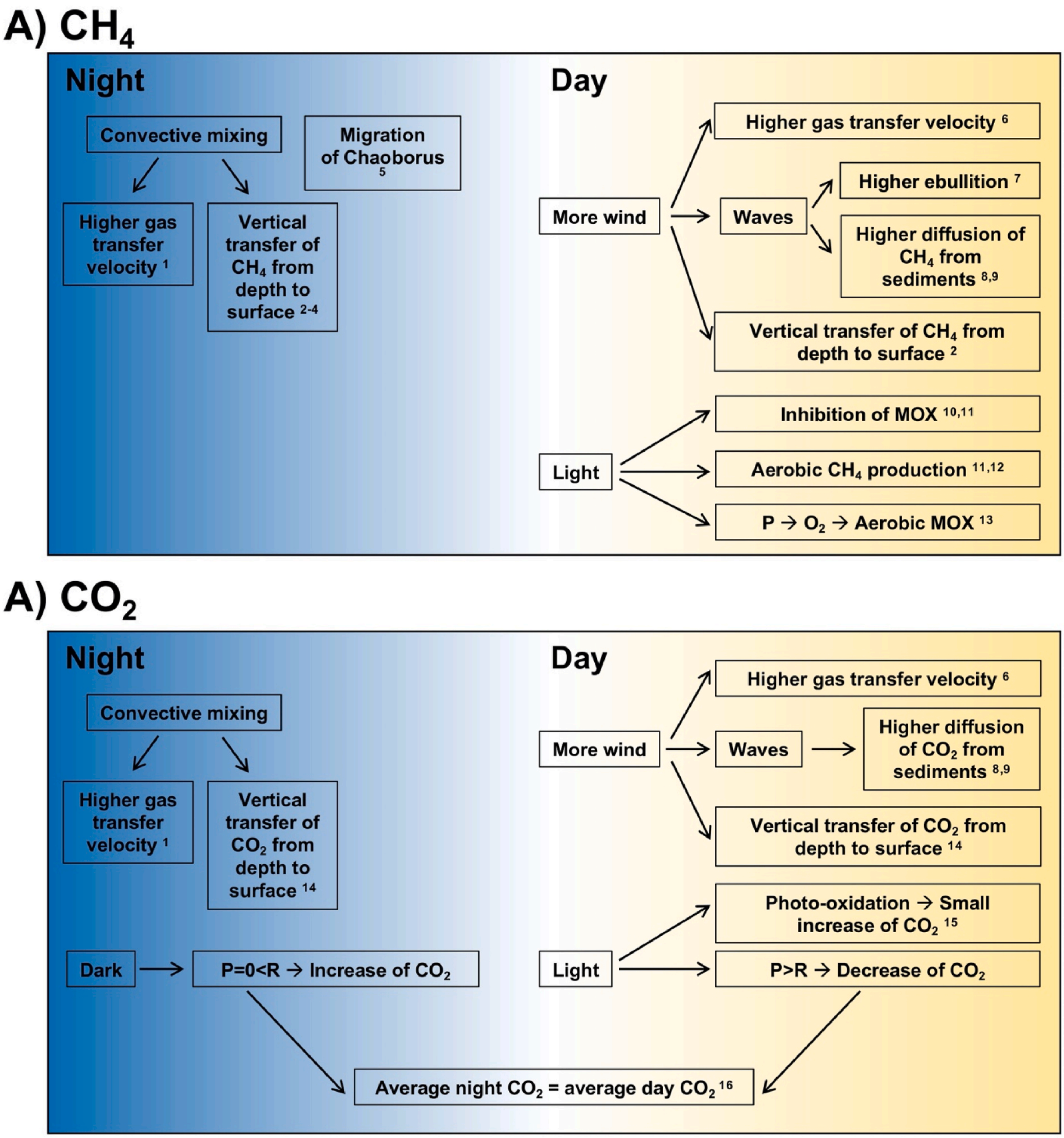

Fig. 1. Diagram summarizing the processes that can increase CH_4 (A) and CO_2 (B) emissions from lakes to the atmosphere during daytime (right) and night-time (left). Available evidence from automated floating domes suggests that the effect of higher daytime wind speed leads to higher CH_4 (Sieczko et al., 2020) and CO_2 (Rudberg et al., 2021) emissions in Swedish lakes. (1) MacIntyre et al. (2010); (2) Sieczko et al. (2020); (3) Martinez-Cruz et al. (2020); (4) Podgrajsek et al. (2014); (5) McGinnis et al. (2017); (6) Wanninkhof (1992); (7) Hofmann et al. (2010); (8) Lorke and Peeters (2006); (9) MacIntyre et al. (2006); (10) Murase and Sugimoto (2005); (11) Morana et al. (2020); (12) Bižić et al. (2020); (13) Oswald et al. (2015); (14) Rudberg et al. (2021); (15) Rocher-Ros et al. (2021) (16) Borges et al. (2022); MOX = methane oxidation; P = gross primary production; R = community respiration.

approaches to derive GHG fluxes has advantages but also limitations that have been documented and several inter-comparisons have evaluated the consistency of the three approaches (e.g. Guérin et al., 2007; Podgrajsek et al., 2014; Holgerson et al., 2017; Erkkilä et al., 2018; MacIntyre et al., 2021a,b). Several processes generate differences in the concentrations of CO_2 and CH_4 and in the *k* values between day-time and night-time resulting in differences in emissions of CO_2 and CH_4 as summarized in Fig. 1. Available evidence from eddy covariance in 13 lakes and reservoirs in the Northern Hemisphere indicated that day-time and night-time CO_2 fluxes were close numerically in 8 systems, but night-time CO_2 fluxes were higher in 5 systems (Golub et al., 2023). Most of the lakes and reservoirs studied by Golub et al. (2023) were located >60°N so the lower average fluxes during day-time could be related to a very long photo-period at higher latitudes during summer when aquatic primary production lowers day-time CO_2 fluxes. Several studies have reported CH_4 flux measurements in lakes with eddy-covariance (Podgrajsek et al., 2014; Franz et al., 2016; Xiao et al., 2017; Jammet et al., 2017; Sollberger et al., 2017; Erkkilä et al., 2018), and approximately half of them reported higher day-time fluxes, and the other half showed higher night-time emissions, as summarized by Sieczko et al. (2020). Available evidence from floating chamber measurements in four Swedish lakes (Sieczko et al., 2020; Rudberg et al., 2021) indicates that both CO_2 and CH_4 emissions tended to be higher during day-time because of higher wind speed leading to higher *k* values (Fig. 1). Under light wind conditions, turbulent kinetic energy can increase during periods of heating (buoyancy flux) related to the establishment of a diurnal thermocline leading to an increase of *k* during the morning till mid-day (MacIntyre et al., 2021a,b). Additionally, higher wind speed during day-time can increase the vertical transfer to surface waters of CO_2 and CH_4 from deep waters rich in these gases, as well as lead to waves that induce pressure variations on sediments and pump pore-waters rich in CO_2 and CH_4 and also induce CH_4 ebullition (Hofmann et al., 2010). During day-time, photosynthesis leads to a decrease of CO_2, although changes of CO_2 during day-time and night-time are generally symmetrical, so that average day-time CO_2 concentration should be nearly identical to average night-time CO_2 concentration if the night-time and day-time periods are similar (~12h:12h). Photo-oxidation of dissolved organic matter can lead to a production of CO_2 during day-time, although this process seems quantitatively modest compared to other processes driving CO_2 variability in lakes (Rocher-Ros et al., 2021). Aerobic CH_4 production seems to be linked directly or indirectly to photosynthesis so it should mainly occur during day-time (Bižić et al., 2020; Morana et al., 2020). Light might additionally inhibit methane oxidation (MOX) (Dumestre et al., 1999; Murase and Sugimoto, 2005; Morana et al., 2020). However, the increase of photosynthetically produced oxygen (O_2) during day-time might favour aerobic MOX at the oxycline (Oswald et al., 2015) as well as superficial sediments in shallow systems. MOX modifies the $^{13}C/^{12}C$ ratio ($\delta^{13}C$-CH_4) of residual CH_4 in water, as methanotrophs preferentially consume CH_4 with the lighter carbon stable isotope (^{12}C) over the heavier one (^{13}C). Altogether these processes might result in CH_4 dissolved concentrations distributed asymmetrically during the diel cycle, possibly higher during day-time, unlike CO_2 concentrations that should be nearly symmetric.

The diel variability of N_2O fluxes in lakes and ponds is less documented than for CO_2 and CH_4. Measurements of CO_2 and CH_4 exchange with the atmosphere can be routinely automated with either eddy-covariance or floating chamber methods coupled to low-cost instrumentation for the latter. This is not the case for N_2O because of lower fluxes (lower signal), inadequate sensitivity or response time of available instrumentation, or unavailability of low cost instrumentation. So, studies of N_2O in lakes and ponds have mostly relied so far on gas chromatography (GC) limiting the possibility of automation. N_2O sources and sinks in lakes depend on denitrification and nitrification that in turn depend on dissolved inorganic nitrogen (DIN) availability and O_2 levels (Mengis et al., 1997; Borges et al., 2023). O_2 levels change in surface waters at daily scale, increasing during day-time with photosynthesis and decreasing during night-time. In shallow systems, these oscillations of O_2 in the water column might modify oxygenation of the top layer of sediments and affect sedimentary processes including nitrification and denitrification. In rivers, a night-time increase of N_2O has been attributed to the lowering of O_2 in the water column (Harrison et al., 2005; Clough et al., 2007; Baulch et al., 2012; Xia et al., 2013; Chen et al., 2021). In Lake Wuliangsuhai (China), Ni et al. (2022) showed that N_2O emissions followed diurnal cycles, peaking in the middle of the day when O_2 concentrations were maximal in areas dominated by submerged macrophytes. Other studies in Lake Taihu (China) (Xiao et al., 2019) and in Ashumet pond (Massachusetts, United states) (Smith et al., 2024) did not report marked and systematic sub-daily changes in N_2O concentrations.

The present paper reports a dataset of CO_2, CH_4, and N_2O dynamics in two contrasted shallow small urban ponds (Pêcheries and Silex) in the city of Brussels (Belgium) (Fig. 2). The Pêcheries pond is a turbid-water phytoplankton dominated system and the Silex pond is a clear-water macrophyte dominated system. The urban ponds in the city of Brussels fall into either of these two categories (Scheffer et al., 1993) that have distinct GHG emission rates (Bauduin et al., 2024a, 2024b). Data were collected every hour starting before dawn and ending after dusk in spring (3rd and 8th April 2023), summer (7th and 13th September 2023), fall (15th and 16th November 2023) and winter (7th and 8th January 2024) at the Pêcheries and the Silex ponds. The objectives of this study are to investigate if diurnal variations in the concentrations and fluxes of CO_2, CH_4, and N_2O (i) are detectable and systematic in the two ponds; (ii) change with season in occurrence or amplitude; (iii) can be explained by biogeochemical processes and/or meteorological conditions such as wind speed or light intensity; (iv) are quantitatively significant compared to seasonal variations in the two ponds and compared to inter-system variation among other ponds of the city of Brussels.

2. Material and methods

2.1. Site description

Belgium is characterized by a temperate climate, with year-round mild temperatures and uniform high precipitation. Over the 1991–2020 period, annual precipitation averaged 837 mm, annual temperature averaged 11 °C, with summer and winter averages of 17.9 °C and 4.1 °C, respectively. The ponds in the city of Brussels are artificial, small, shallow, and eutrophicated (De Backer et al., 2010; Van Onsem et al., 2010; Peretyatko et al., 2012). The ponds in the periphery of the city are located in the Sonian Forest, the ponds closer to the city center are situated primarily within recreational parks. Several ponds of the city of Brussels are located in protected Natura 2000 areas and are valuable for biodiversity conservation, as well as for recreational purposes such as boating and fishing. The ponds in the city of Brussels are eutrophic, and occur in two states *sensu* Scheffer et al. (1993): clear-water ponds with dominance of a few macrophyte species with a variable abundance (Peretyatko et al., 2007); turbid-water ponds with dominance of phytoplankton composed mainly of cyanobacteria with occasional harmful algal blooms (De Backer et al., 2010; Van Onsem et al., 2010; Peretyatko et al., 2012). The accumulation of high cyanobacteria biomass can lead to anoxic/hypoxic conditions and/or accumulation of toxins causing occasional fish kills, with a negative effect on the aquatic ecological functioning and leading to public health concerns (De Backer et al., 2010; Van Onsem et al., 2010; Peretyatko et al., 2012).

The two sampled ponds (Pêcheries and Silex) are located in the city of Brussels, in the Woluwe river basin, at the periphery of the Sonian forest (Fig. 2). The Pêcheries and the Silex ponds are both relatively small (1.0–1.4 ha) and shallow (1.1–1.3 m) (Fig. 2), and mainly differ in the type of dominant aquatic primary producer during spring-summer. The Pêcheries pond is a turbid-water pond with higher chlorophyll-*a* (Chl-*a)* and total suspended matter (TSM) values during summer (Fig. 2)

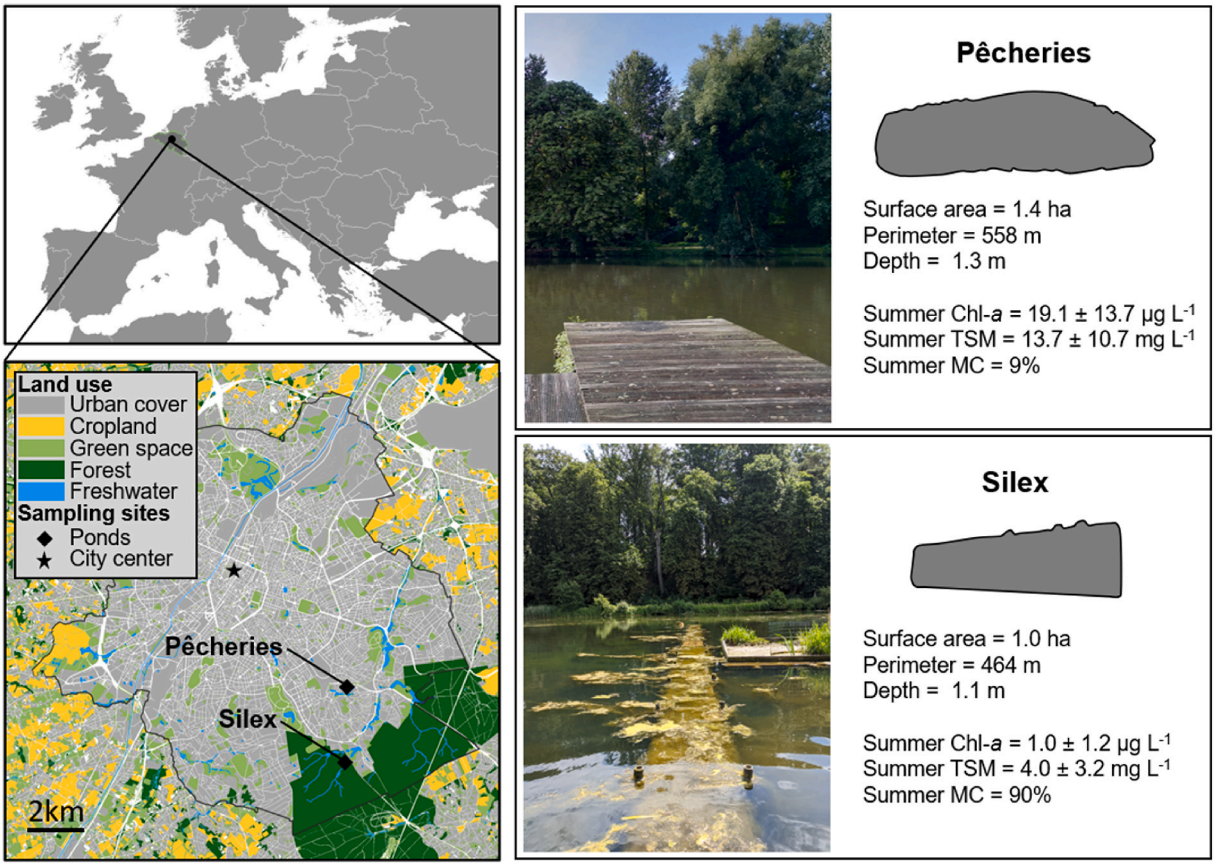

Fig. 2. Location of the two sampled ponds in Brussels (Belgium, Europe). Bottom left map shows the metropolitan area of the region of Brussels delineated by the black line and surrounding region of Flanders in Belgium, showing land cover and sampled urban ponds (black diamonds). The star corresponds to the center of the city (50.8504°N, 4.3487°E). Additional information for each pond is indicated on right panels: shapes of the ponds, surface area (ha), perimeter (m), average depth (m) (obtained thanks to Bruxelles Environnement, the regional water management agency), mean ± standard deviation of summer chlorophyll-*a* (Chl-*a*, µg L^{-1}) and summer total suspended matter (TSM, mg L^{-1}) of periods from 21 June to 21 September in 2021, 2022, 2023, and summer total macrophyte cover (MC, %) from Bauduin et al. (2024a).

due to a dominance of aquatic primary production by phytoplankton (mainly cyanobacteria). The Silex pond is a clear-water pond with lower Chl-*a* and TSM values due to a dominance of aquatic primary production by submerged macrophytes (mainly *Lemna trisulca*). The seasonal and inter-annual variations of CO_2, CH_4, and N_2O dissolved concentrations and emissions were reported in two companion papers (Bauduin et al., 2024a, 2024b), but information on variations at sub-daily scale were lacking, so their relative importance is unknown.

2.2. Meteorological data

Hourly data acquired by the Royal Meteorological Institute of Belgium of air temperature, rainfall, wind speed, and atmospheric pressure referenced at 10m height were retrieved from https://wow.meteo.be/en for the meteorological station closest to the two ponds (Institute of St-Lambert; 50.8408°N 4.4234°E) located 2.5 km away from the Pêcheries pond and 5 km way from the Silex pond. Hourly data of solar irradiance referenced at 37m height and corrected for cloud cover and aerosols were retrieved from the Prediction Of Worldwide Energy Resources Data Archive (https://power.larc.nasa.gov/) for the same location. The hourly data of solar irradiance were integrated at daily scale using the trapezoidal method. The meteorological data are used to contextualize the differences of the patterns of sub-daily variations of CO_2, CH_4, and N_2O concentrations and fluxes between the two ponds and between seasons. Wind speed is also used to compute the *k* values from a *k*-wind parameterization (section 2.5).

2.3. Sampling strategy and field sampling

Sampling was designed to investigate sub-daily variability of GHG concentrations and was not designed to describe spatial variability within the ponds (assumed low since the ponds are small and uniformly shallow), so sampling was carried out at a single location. Two ponds were investigated to test if sub-daily variability changed among clear-water and turbid-water ponds. Four sampling periods were chosen (03–08/04/2023, 07–13/09/2023, 15–16/11/2023, 07–08/01/2024) to test if the patterns and the amplitude of sub-daily variations changed with season (spring, summer, fall, and winter, respectively). Sampling was carried out at a single location, from a pontoon, every hour, starting 1–2h hour before dawn and ending 2–3h after dusk.Water was collected manually 5 cm below the surface with seven polypropylene syringes (60 ml) for gases (CO_2, CH_4, N_2O). Prior to sampling, the syringes were rinsed three times with surface water. Water was sampled taking care to avoid the inclusion of air bubbles, to prevent the alteration of the content of dissolved gases. After sample collection, the syringes were processed as quickly as possible to minimize biological alteration of the content of dissolved gases. Three syringes were used to preserve water samples for subsequent analysis of CH_4 and N_2O, and $\delta^{13}C$-CH_4 in the laboratory and four syringes were used to measure the partial pressure of CO_2 (pCO_2) directly in the field. The water was transferred, taking care to avoid the inclusion of air bubbles, from the syringes with a polyvinyl chloride flexible tube (Tubclair®) into three 60 ml borosilicate serum bottles (Wheaton™) for CH_4 and N_2O, and $\delta^{13}C$-CH_4, preserved with 200 µl of a saturated solution of $HgCl_2$, sealed with a butyl stopper without a headspace and crimped with an aluminium cap, for subsequent analysis at the laboratory. The pCO_2 measurements were carried out directly in the field with a Li-Cor® Li-840 CO_2/H_2O gas analyser using the headspace technique in four syringes by equilibrating 30 ml of sample water with 30 ml of atmospheric air by vigorous shaking during 5 min (Borges et al., 2019). The Li-Cor® Li-840 was calibrated 1–2 days before each sampling with ultrapure N_2 and a suite of gas standards (Air Liquide™ Belgium) with CO_2 mixing ratios of 388, 813, 3,788, and 8300 ppm manufactured and certified at ±2% by Air Liquide™ Belgium. The 388 ppm and 813 ppm CO_2 gas standards from Air Liquide™ Belgium were recalibrated against CO_2 standard reference materials (SRM) traceable to United States of America National Institute of Standards and Technology (NIST) reference materials provided by the National Oceanic and Atmospheric Administration (NOAA) with CO_2 mixing ratios of 360.5 and 773.8 ppm. Drift in the calibration of the Li-Cor® Li-840 was checked by measuring the standards again after each sampling within 1–2 days, and was systematically undetectable (within the precision of instrument). The overall precision of pCO_2 measurements was ±2.0% with a detection limit of 5 ppm.

Water temperature (precision ±0.1 °C), specific conductivity (precision ±0.1 μS cm^{-1}), and O_2 saturation level (%O_2) (precision ±0.1%) were also measured in-situ simultaneously every hour with a VWR® MU 6100H probe. The O_2 probe was calibrated in humidity saturated ambient air at the start of the experiment following the manufacturer recommendation. The conductivity probe was calibrated with a commercial standard (Merck®) of 1000 μS cm^{-1} (United Nations Standard Products and Services (UNSPSC) Code 41,116,107). Polyethylene containers (2l) were filled with water three to four times a day, stored in cool boxes with frozen packs and processed at the laboratory for soluble reactive phosphorus (SRP), ammonium (NH_4^+), nitrite (NO_2^-), nitrate (NO_3^-), Chl-*a*, and TSM concentrations. Prior to sampling, the polyethylene container was rinsed three times with surface water.

2.4. Laboratory analysis

2.4.1. CH_4 and N_2O measurements by gas chromatography and $\delta^{13}C$-CH_4 by cavity ring-down spectrometry

Measurements of N_2O and CH_4 dissolved concentrations were made with the headspace technique (Weiss, 1981) and a GC, following standard operating procedures to quantify GHG emissions from inland waters (UNESCO/IHA, 2010). The used instrumental set-up and analytical protocol compared satisfactorily with 14 other laboratories during an international inter-comparison exercise of CH_4 and N_2O measurements (Wilson et al., 2018). The headspace (20 ml) was made with ultra-pure N_2 (Air Liquide™ Belgium) in two 60 ml serum bottles for a replicate analysis of both CH_4 and N_2O.The GC (SRI™ 8610C) was equipped with a flame ionisation detector for CH_4 and an electron capture detector for N_2O, and was calibrated with CH_4:N_2O:N_2 gas mixtures with mixing ratios of 1, 10 and 30 ppm for CH_4, and 0.2, 2.0 and 6.0 ppm for N_2O, manufactured and certified at ±2% for CH_4 and ±10% for N_2O by Air Liquide™ Belgium. The precision of measurements based on duplicate samples was ±3.9% for CH_4 and ±3.2% for N_2O. The detection limit was 0.5 nmol L^{-1} for both CH_4 and N_2O.

The CO_2 concentration is expressed as partial pressure in parts per million (ppm) and CH_4 as dissolved concentration (nmol L^{-1}), in accordance with convention in existing topical literature, and because both quantities were systematically and distinctly above saturation level (~400 ppm and 2–3 nmol L^{-1}, respectively). Variations of N_2O fluctuated around atmospheric equilibrium, so data are presented as percent of saturation level (%N_2O, where atmospheric equilibrium corresponds to 100%).

The $\delta^{13}C$-CH_4 was measured in the headspace gas (20 ml of synthetic air, Air Liquide™ Belgium) equilibrated with the water sample (total volume 60 ml) on a single serum bottle. All of the samples had a headspace with a partial pressure of CH_4 (pCH_4) higher than 10 ppm, so the gas samples were diluted to achieve a final pCH_4 around 6 ppm to fall within instrumental operational concentration range (2–10 ppm) recommended by the manufacturer. The diluted gas was then injected into a cavity ring-down spectrometer (Picarro™ G2201-i, isotopic analyzer) equipped with a Small Sample Introduction Module 2 (Picarro™). The data were corrected using calibration curves of $\delta^{13}C$-CH_4 as a function of concentration, based on two gas standards from Airgas™ Specialty Gases with certified $\delta^{13}C$-CH_4 values of −23.9 ± 0.3 ‰ and −69.0 ± 0.3 ‰ referenced against Vienna Pee Dee Belemnite SRM. The precision of measurement based on repeated analysis of the two standards was better than ±1.0 ‰.

2.4.2. Chlorophyll-a, total suspended matter, and dissolved inorganic nutrients

Chl-*a*, TSM, and dissolved inorganic nutrients (SRP, NH_4^+, NO_2^-, NO_3^-) were measured using standard operating procedures for the analysis of water quality (APHA, 1998) by fluorimetry, differential weight, and colorimetric-spectrophotometric measurements, respectively. A known volume of water was filtered through Whatman™ GF/F glass microfiber filters (porosity 0.7 μm) with a diameter of 47 mm for Chl-*a* and TSM determination. Filters were kept frozen (−20 °C) until extraction of Chl-*a* in 90% acetone and the measurement of the concentration by fluorimetry with a Kontron™ model SFM 25 according to Yentsch and Menzel (1963), with a precision of ±0.1 μg L^{-1} and detection limit of 0.05 μg L^{-1}. A calibration curve was made from sequential dilutions with 90% acetone of a commercial (Merck®) Chl-*a* standard (UNSPSC Code 41,116,107). Filters used for the determination of TSM were weighed with a Explorer™ Pro EP214C analytical microbalance with ±0.1 mg precision scale after oven drying at 50 °C during 12h before and after filtration of a known volume of water, with a precision of ±10% and detection limit of 0.05 mg L^{-1}. Filtered water for the determination of dissolved nutrients was stored frozen (−20 °C) in 50 ml polypropylene vial. Absorption measurements for the colorimetric determination of dissolved nutrients were made with a Perkin Elmer™ Lambda 650S spectrophotometer. SRP was measured by the ammonium molybdate, ascorbic acid, and potassium antimony tartrate staining method (Koroleff, 1983). NH_4^+ was measured by the nitroprusside-hypochlorite-phenol staining method (Grasshoff and Johannsen, 1972). NO_2^- and NO_3^- were measured before and after reduction of NO_3^- to NO_2^- by a cadmium-copper column, using the Griess acid reagent staining method (Grasshoff et al., 2009). Calibration curves were made from sequential dilutions with pure water of commercial standards (Merck®) traceable to NIST SRMs (84L for PO_4^{3-}, 999b for NH_4^+, 8040 for NO_2^-, 723 for NO_3^-). Precisions were ±0.05, ±0.02, ±0.02, and ±0.1, μmol L^{-1} for SRP, NH_4^+, NO_2^-, and NO_3^-, respectively. Detection limits were 0.01, 0.3, 0.01, and 0.15 μmol L^{-1} for SRP, NH_4^+, NO_2^-, and NO_3^-, respectively.

2.5. Calculation of diffusive GHG emissions

The diffusive air-water CO_2, CH_4, or N_2O fluxes (F_G) were calculated according to eq. (1):

$$F_G = k\,\Delta[G] \tag{1}$$

where k is the gas transfer velocity and Δ[G] is the air-water gas concentration gradient. Δ[G] was computed from the measured dissolved concentrations of CO_2, CH_4, and N_2O and from dissolved concentrations at equilibrium with the partial pressure in air of the respective gases using the Henry constants computed from water temperature using the algorithms of Weiss (1974) for CO_2, Yamamoto et al. (1976) for CH_4, and Weiss and Price (1980) for N_2O. The atmospheric pCO_2 was measured on the field with the Li-Cor Li-840. For CH_4, the global average present day atmospheric mixing ratio of 1.9 ppm was used (Lan et al., 2024). The monthly global average air mixing ratios of N_2O provided by the Global Monitoring Division of the NOAA Earth System Research Laboratory (Dutton et al., 2017) were used. k was computed from a value normalized to a Schmidt number of 600 (k_{600}) and from the Schmidt number of CO_2, CH_4 and N_2O in freshwater computed from water temperature with the algorithms given by Wanninkhof (1992). k_{600} was calculated from the parameterization as a function of wind speed of Cole and Caraco (1998) that was chosen for consistency and comparability with two companion papers on GHG emissions from urban ponds in the city of Brussels (Bauduin et al., 2024a, 2024b). The k_{600}-wind parametrization of Cole and Caraco (1998) intrinsically integrates other sources of turbulence such as night-time convection due to cooling and the effect of fetch limitation, because it is derived from a large compilation of repeated tracer measurements in 11 lakes with a wide range of surface area (0.2–487 km^2) and maximum depth (1–109m).

2.6. *Statistical analysis*

Statistical analyses were carried out with R package version 4.4.1 (R Core Team, 2021). Relationships between variables were evaluated by linear regression, using the coefficient of determination (r^2) to measure correlation strength and Fisher's F test and the associated *p*-value to

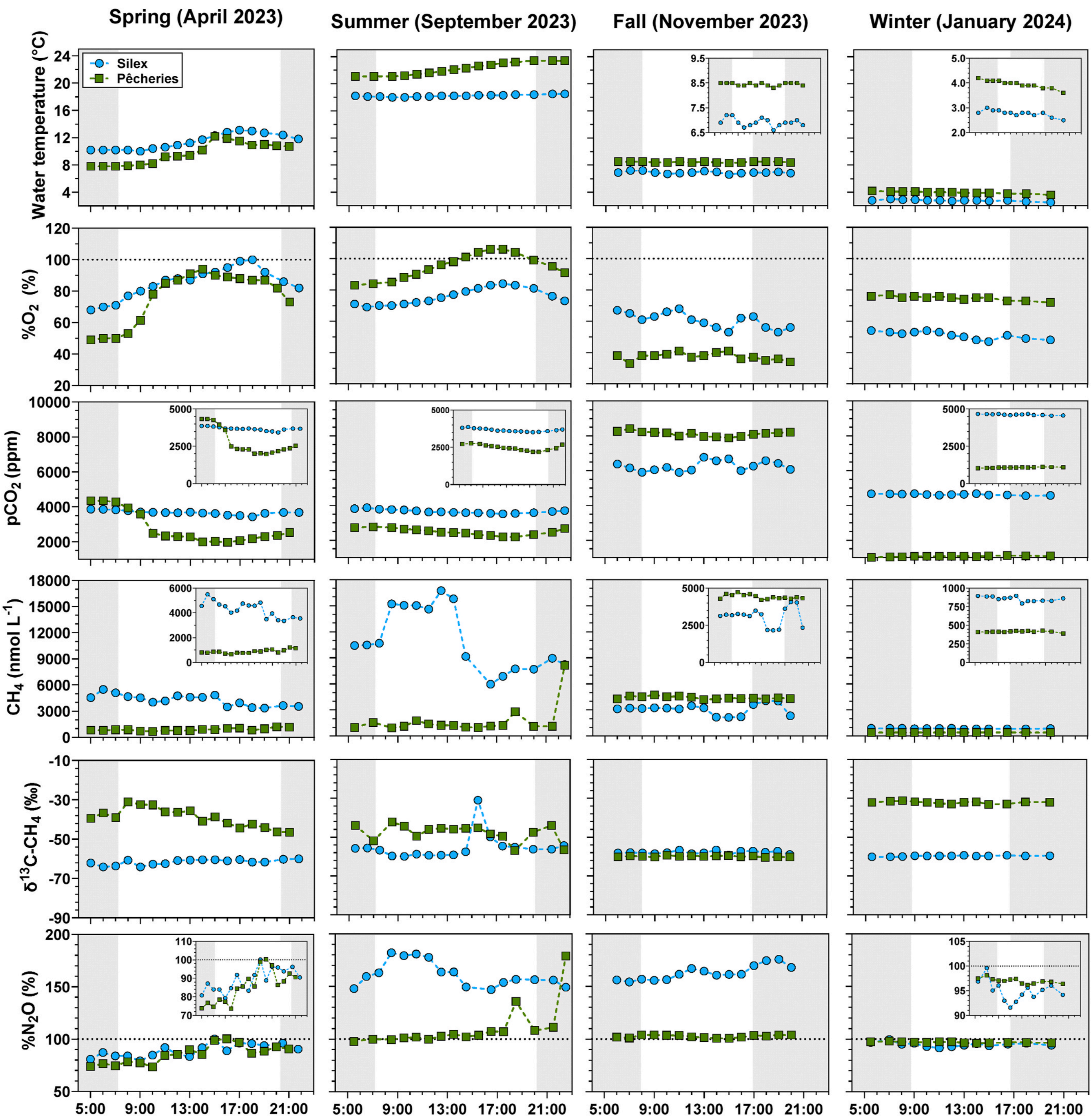

Fig. 3. Hourly measurements of water temperature (°C), oxygen saturation level (%O_2, in %), partial pressure of CO_2 (pCO_2, in ppm), dissolved CH_4 concentration (CH_4, in nmol L^{-1}), $^{13}C/^{12}C$ ratio of CH_4 in surface waters ($\delta^{13}C$-CH_4, in ‰) and N_2O saturation level (%N_2O, in %) in spring (3rd and 8th April 2023), summer (7th and 13th September 2023), fall (15th and 16th November 2023) and winter (7th and 8th January 2024) at the Pêcheries and Silex ponds in Brussels, respectively. The vertical grey bands represent times of day before sunrise and after sunset.

measure statistical significance. Differences in GHG fluxes between three periods of the day (late night, mid-day, and early night) were tested with Tukey's honestly significant difference post-hoc test following one-way repeated measures analysis of variance (ANOVA).

The abbreviations used in this work are listed and defined in Table S1.

The data supporting this study are available at https://zenodo.org/records/11395489

3. Results and discussion

3.1. Variations of meteorological conditions and GHG concentrations at sub-daily scale

The seasonal range of recorded air temperature for all sub-daily samplings at the two urban ponds in the city of Brussels was from −2.8 °C in winter to 30.3 °C in summer (Fig. S1). The amplitude between the minimum and the maximum values of air temperature variations during individual sub-daily samplings was minimal in winter (1.4 °C at the Silex pond) and maximal in summer (13.6 °C at the Pêcheries pond). During sub-daily samplings in both ponds, precipitation did not occur in spring and summer, low precipitation occurred in winter, and higher precipitation occurred in fall in particular during the sampling of the Silex pond (Fig. S1). In both ponds, wind speed was generally low (≤4 m s^{-1}) in spring and summer, and higher in fall and winter with maximum values > 5 m s^{-1} (except at the Pêcheries pond in winter with wind speed <2 m s^{-1}). In spring, summer, and fall, wind speed was usually higher at the middle of the day than at dawn and dusk. In winter, wind speed increased regularly from dawn to dusk at the Pêcheries pond and was relatively constant at the Silex pond (Fig. S1).

The seasonal range of water temperature for all sub-daily samplings in both ponds was from 2.5 °C in winter to 23.4 °C in summer (Fig. 3). The amplitude of water temperature sub-daily variations was minimal in winter and fall (≤0.6 °C) and maximal in spring (4.4 °C at the Pêcheries pond and 3.1 °C at the Silex pond). The turbid-water Pêcheries pond was characterized by high Chl-*a* (19.1 ± 13.7 μg L^{-1}) and TSM (13.7 ± 10.7 mg L^{-1}) values while the clear-water Silex pond was characterized by low Chl-*a* (1.0 ± 1.2 μg L^{-1}) and TSM (4.0 ± 3.2 mg L^{-1}) values (Fig. 2 and Table 1). The comparison of average Chl-*a* during the sub-daily samplings with the seasonally resolved higher data-density time series reported by Bauduin et al. (2024a) showed that the sampling in September at the Pêcheries pond occurred after the peak of phytoplankton in August, but that the Chl-*a* values were consistent on the other three occasions, as well on all four occasions at the Silex pond where Chl-*a* values were uniformly low during the year (Fig. S2). The seasonal range of SRP concentrations for all sub-daily samplings in both ponds was from 0.5 to 5.5 μmol L^{-1} and concentrations peaked in fall in both ponds (Table 1). The measured SRP concentrations were higher during each season at the Silex pond. The seasonal range of NH_4^+ concentrations for all sub-daily samplings in both ponds was from 0.9 to 11.0 μmol L^{-1}, with maximal values in fall and minimal values in summer in both ponds (Table 1). The seasonal range of NO_2^- concentrations for all sub-daily samplings in both ponds was from 0.1 to 3.3 μmol L^{-1}, with maximal values in fall in both ponds (Table 1). The seasonal range of NO_3^- concentrations for all sub-daily samplings in both ponds was from 6.1 to 28.8 μmol L^{-1}, with maximal values in fall at the Silex pond and in winter at the Pêcheries pond (Table 1). The TSM, Chl-*a*, SRP, NH_4^+, NO_2^-, and NO_3^- data collected at sub-daily scale from this study were within the range and the means were comparable to the respective seasonal data from Bauduin et al. (2024a) in the same ponds based on a dense seasonal sampling from June 2021 to December 2023 (once a day from one (winter) to three (summer) times per month) (Table S2).

The seasonal range of %O_2 for all sub-daily samplings was from 33% in fall to 106% in summer, at the Pêcheries pond (Fig. 3). The amplitude of %O_2 sub-daily variations was minimal in winter (≤7% at both ponds) and highest in spring (45% at the Pêcheries pond and 32% at the Silex pond). In spring and summer, %O_2 followed a temporal pattern consistent with diel variations of photosynthesis with a gradual increase from dawn to mid-afternoon followed by a gradual decrease until dusk (Fig. 3). In fall and winter, %O_2 decreased during the course of the sampling at both ponds, expect in fall at the Pêcheries pond when %O_2 variations were erratic.

The seasonal range of pCO_2 for all sub-daily samplings was from 1026 ppm in winter to 8417 ppm in fall at the Pêcheries pond in both cases (Fig. 3). The pCO_2 values were systematically above atmospheric equilibrium (~400 ppm) showing that both ponds acted as sources of CO_2 to the atmosphere whatever the time of the day and whatever the season. The amplitude of pCO_2 sub-daily variations was minimal in winter (≤120 ppm at both ponds) and highest in spring (2373 ppm at the Pêcheries pond and 440 ppm at the Silex pond). The amplitude of sub-daily variations of pCO_2 was highest in spring probably due to more favourable light conditions for photosynthesis that led to the onset of the spring phytoplankton bloom in the Pêcheries pond and the growth of

Table 1
Daily mean ± standard deviation of soluble reactive phosphorus concentration (SRP, in μmol L^{-1}), ammonium concentration (NH_4^+, in μmol L^{-1}), nitrite concentration (NO_2^-, in μmol L^{-1}), nitrate concentration (NO_3^-, in μmol L^{-1}), chlorophyll-*a* concentration (Chl-*a*, in μg L^{-1}), and total suspended matter concentration (TSM, in mg L^{-1}) measured at the Pêcheries and Silex ponds in the city of Brussels for the four seasons, from samples collected three times a day (in the morning, noon, and end of the day), and daily integrated solar irradiance (in W m^{-2}). Table S2 provides a comparison of the means and minimum and maximum range of sub-daily measurements from this study and seasonal data from Bauduin et al. (2024a) based on sampling once a day from one (winter) to three (summer) times per month from June 2021 to December 2023.

Season	Date	Pond	SRP (μmol L^{-1})	NH_4^+ (μmol L^{-1})	NO_2^-(μmol L^{-1})	NO_3^-(μmol L^{-1})	Chl-*a* (μg L^{-1})	TSM (mg L^{-1})	Daily solar irradiance (W m^{-2})
Spring 2023	03-04-23	Pêcheries	0.5 ± 0.1	4.9 ± 0.6	0.2 ± 0.0	10.4 ± 3.0	5.5 ± 0.3	4.3 ± 0.9	2471
	08-04-23	Silex	1.0 ± 0.2	2.7 ± 0.5	0.1 ± 0.0	7.3 ± 0.8	0.9 ± 0.1	1.6 ± 0.3	2344
Summer 2023	07-09-23	Pêcheries	1.6 ± 0.3	0.9 ± 0.5	0.3 ± 0.0	6.1 ± 0.7	14.5 ± 1.1	27.1 ± 2.1	3403
	13-09-23	Silex	3.8 ± 0.5	2.7 ± 0.2	0.8 ± 0.3	10.7 ± 0.2	1.2 ± 0.1	2.9 ± 0.5	2651
Fall 2023	15-11-23	Pêcheries	1.6 ± 0.2	2.7 ± 0.2	0.7 ± 0.1	7.6 ± 0.8	14.8 ± 1.5	19.0 ± 1.5	482
	16-11-23	Silex	5.5 ± 0.2	11.0 ± 0.7	3.3 ± 0.5	28.8 ± 2.5	6.9 ± 0.9	9.2 ± 1.9	509
Winter 2024	07-01-24	Pêcheries	0.7 ± 0.2	5.9 ± 0.3	0.3 ± 0.0	15.9 ± 0.8	2.7 ± 0.7	13.4 ± 2.4	403
	08-01-24	Silex	0.8 ± 0.2	5.6 ± 0.3	1.6 ± 0.2	19.4 ± 0.9	0.6 ± 0.1	8.6 ± 1.4	456

macrophytes in the Silex pond. Indeed, daily solar irradiance values in spring were higher than in fall and winter but lower than in summer (Table 1). The sub-daily sampling in summer in the Pêcheries pond was carried out after the phytoplankton peak in August (Fig. S2). Consequently, despite higher daily solar irradiance values in summer than spring (Table 1), the amplitude of sub-daily variations of pCO_2 (351 ppm) in the Pêcheries pond was lower in summer during senescence of the phytoplankton bloom than in spring (2373 ppm) during presumably the onset of the spring phytoplankton bloom. In spring and summer, pCO_2 followed a temporal pattern consistent with diel variations of photosynthesis as function of light with a gradual decrease from dawn to mid-afternoon followed by a gradual increase until dusk. This was consistent with $\%O_2$ variations mirroring the pCO_2 variations in spring and summer (Fig. 3). The daily photosynthesis cycle is presumably due to phytoplankton in the Pêcheries pond and macrophytes in the Silex pond. In fall at the Pêcheries pond, pCO_2 also followed the cycle expected from daily variations of photosynthesis, but not at the Silex pond where pCO_2 showed erratic variations. In winter, pCO_2 increased and decreased during day-time at the Pêcheries pond and at the Silex pond, respectively (Fig. 3), but these changes were marginal compared to other seasons, with amplitudes of pCO_2 sub-daily variations of 121 ppm at the Silex pond and 93 ppm at the Pêcheries pond.

The seasonal range of CH_4 dissolved concentration for all sub-daily samplings in both ponds was from 391 nmol L^{-1} in winter at the Pêcheries pond to 16,736 nmol L^{-1} in summer at the Silex pond (Fig. 3). The CH_4 dissolved concentration values were systematically above atmospheric equilibrium (2–3 nmol L^{-1}) showing that both ponds acted as sources of CH_4 to the atmosphere whatever the time of the day and whatever the season. During all seasons, the CH_4 dissolved concentrations were higher at the Silex pond than the Pêcheries pond (Table S2) in agreement with the previously reported pattern across 22 urban ponds in the city of Brussels showing higher CH_4 emissions in clear-water ponds than turbid-water ponds (Bauduin et al. 2024a, 2024b). The amplitude of sub-daily variations of CH_4 dissolved concentration was minimal in winter ($\leq$103 nmol L^{-1} in both ponds) and highest in summer (7186 nmol L^{-1} at the Pêcheries pond and 10,774 nmol L^{-1} at the Silex pond). Sub-daily variations in CH_4 dissolved concentrations did not correlate with the sub-daily variations in water temperature. The amplitude of water temperature variations at sub-daily scale (0.5 °C in winter to 2.6 °C in summer) were small compared to the seasonal scale (23.5 °C) for which a dependence between CH_4 concentrations and temperature was reported in these two ponds (Bauduin et al., 2024a). For most samplings, the CH_4 dissolved concentrations did not show a discernible temporal pattern during day-time and variations were erratic (with a few exceptions, see hereafter). These erratic temporal patterns of CH_4 dissolved concentrations were mirrored by variations of

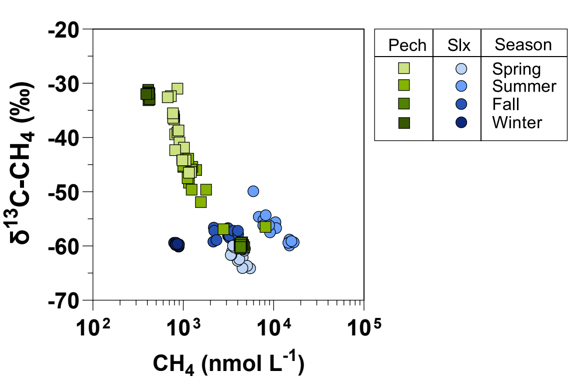

Fig. 4. Hourly measurements of $^{13}C/^{12}C$ ratio of CH_4 in surface waters ($\delta^{13}C$-CH_4, in ‰) versus dissolved CH_4 concentration (CH_4, in nmol L^{-1}) in spring (3rd and 8th April 2023), summer (7th and 13th September 2023), fall (15th and 16th November 2023) and winter (7th and 8th January 2024) at the Pêcheries (Pech) and Silex (Slx) ponds in Brussels, respectively.

$\delta^{13}C$-CH_4 (Figs. 3 and 4). This suggests that CH_4 dissolved concentration and $\delta^{13}C$-CH_4 resulted from spurious changes in balance of the removal of CH_4 in the water column by MOX and degassing to the atmosphere and inputs of CH_4 fluxing out of the sediment. The CH_4 fluxing out of the sediment is itself also partly function of MOX at the sediment-water interface and in the superficial oxic sediment layer, and of methanogenesis deeper in the sediment.

At the Pêcheries pond, in spring, CH_4 dissolved concentrations showed a regular pattern, with an increase of values during day-time that could be related to an increase of light limitation of MOX (Dumestre et al., 1999; Murase and Sugimoto, 2005; Morana et al., 2020). The intensity and amplitude of variations of light during the day were highest in spring and summer, which also corresponded to the largest variations in $\delta^{13}C$-CH_4 observed in both ponds (4.8 ‰ and 1.4 ‰ in spring, and 4.3 ‰ and 6.8 ‰ in summer, compared to 0.3 ‰ and 0.8 ‰ in fall, and 0.6 ‰ and 0.2 ‰ in winter at the Pêcheries pond and the Silex pond, respectively).

The relatively strong decrease of CH_4 dissolved concentration observed between morning and afternoon at the Silex pond in spring (decrease of 2169 nmol L^{-1}) and summer (decrease of 10,774 nmol L^{-1}) occurred as $\%O_2$ increased in the water column. Higher O_2 in the water column should lead to a higher diffusion of O_2 into the top layer of the sediment enhancing MOX and decreasing the CH_4 fluxing from the sediment, resulting in a lowering of CH_4 dissolved concentration in surface waters.

In summer at the Pêcheries pond, CH_4 dissolved concentrations were relatively uniform from dawn to 17:30 (950–1798 nmol L-1) and at 18:30 suddenly increased by 1555 nmol L^{-1}, and increased again at 22:30 by 7000 nmol L^{-1}. These two sharp increases of CH_4 dissolved concentrations coincided with decreases of $\delta^{13}C$-CH_4 and, more surprisingly, with equally sharp increase in $\%N_2O$ (Fig. 3). Water temperature was comparatively high during this sampling (up to 23.5 °C), favourable to ebullition from the sediments that was shown to be positively related to water temperature in shallow ponds including urban ponds of the city of Brussels (Bauduin et al., 2024a). The strong temperature increase during day-time, as well as a decrease of atmospheric pressure (Fig. S1), were probably very favourable to ebullition at the end of the day during the sampling in summer at the Pêcheries pond. The high temperature was probably more important in triggering ebullition than change in atmospheric pressure that seems to be important in driving ebullition only at low temperatures in these ponds (Bauduin et al., 2024a). Additionally, the drop in atmospheric pressure was modest compared to other sampling periods when more important changes in atmospheric pressure were observed but without a sharp increase of CH_4 dissolved concentrations (Fig. S1). Ebullition could have directly increased CH_4 dissolved concentrations in the water column through dissolution of rising bubbles (McGinnis et al., 2016). Additionally, it is hypothesized that the physical disruption of the sediments by bubbling also contributed to mix pore water rich in CH_4 and N_2O contributing to the observed peaks of these two gases (e.g. Liikanen et al., 2002).

In both ponds, the variations of CH_4 dissolved concentration in surface waters during the course of the day in fall and winter did not follow the pattern observed in summer and spring, possibly due to lower methanogenesis related to lower temperatures and lower fluxing of CH_4 from sediments, as well as a lower increase of O_2 in the water column during day-time, and lower light intensities susceptible of inducing light limitation of MOX. The decrease of CH_4 dissolved concentration observed between morning and afternoon at the Pêcheries pond in fall (decrease of 520 nmol L^{-1}) and at the Silex pond in winter (decrease of 103 nmol L^{-1}) occurred as $\%O_2$ decreased as well in the water column. These variations of CH_4 dissolved concentration could have been erratic as it was the case in other occasions (the Silex pond in fall and the Pêcheries pond in winter).

The seasonal range of $\%N_2O$ variations for all sub-daily samplings was from 73.6% in spring at the Pêcheries pond to 182.0% in summer at the Silex pond (Fig. 3). %N_2O oscillated around saturation (100%) showing these ponds acted alternatively as sinks or sources of N_2O.The amplitude of %N_2O sub-daily variations was minimal in winter (≤8.0 % in both ponds) and maximal in summer (81.2% at the Pêcheries pond and 34.9% at the Silex pond). The very high daily amplitude in summer at the Pêcheries pond (81.2%) could be related to high inputs of N_2O from sediments putatively due to an ebullition event (see above) that caused physical disruption of the sediments, leading to the mixing of pore-waters with bottom pond waters, promoting the transport of DIN and N_2O to the upper part of the water column (e.g. Liikanen et al., 2002). The %N_2O levels were generally close to saturation, with notable deviations during summer and fall at the Silex pond, when higher %N_2O values were observed. These higher %N_2O levels coincided with periods of high NH_4^+ concentrations at the Silex pond (Table S2) and could have resulted from enhanced nitrification as suggested by equally high NO_2^- values. In spring at both ponds and in summer at the Pêcheries pond (excluding the two extreme peaks of %N_2O), %N_2O increased during the day in parallel to %O_2, and %N_2O was positively correlated to %O_2 (Fig. S3). This pattern is unexpected as N_2O is usually negatively related to O_2 in aquatic environments rich in DIN (e.g. Rosamond et al., 2012), although in DIN poor environments a positive relation can emerge, most probably related to N_2O removal by denitrification (e.g. Borges et al., 2018, 2019, 2022, 2023), which is unlikely in the DIN rich eutrophic sampled ponds. A possible explanation of the positive relationship between %N_2O and %O_2 is that an increase of O_2 in the water column led to a transfer of O_2 to sediments and enhanced nitrification leading to an increase of N_2O production. Alternatively, N_2O could have been produced by microalgae themselves (Weathers, 1984; Guieysse et al., 2013; Burlacot et al., 2020; Plouviez et al., 2017, 2019, 2020; Fabisik et al., 2023). This could explain the day-time increase of %N_2O in summer and spring at the Pêcheries pond where Chl-*a* was more abundant (Table 1) than at the Silex pond. At the Silex pond, phytoplankton was less abundant (Table 1) and the macrophyte *Lemna trisulca* was dominant. Yet, higher plants can also produce N_2O (Lenhart et al., 2019), so the daytime increase of %N_2O in Silex in spring could in theory be also linked to primary production leading to a parallel increase with %O_2.

In summer and fall at the Silex pond, a negative relationship between %N_2O and %O_2 was observed (Fig. S3), a common feature in aquatic environments rich in DIN (e.g. Rosamond et al., 2012) including rivers in Belgium (Borges et al., 2018). The negative relationship between %N_2O and %O_2 probably reflected an increase in the yield of N_2O production by nitrification at lower O_2 levels (Goreau et al., 1980; Ni et al., 2011). Additionally, low %O_2 conditions reflect higher organic matter degradation at community level, hence, also NH_4^+ production by ammonification, leading to higher rates of nitrification and N_2O production. Indeed, the highest daily %N_2O values observed in summer and fall at the Silex pond coincided with higher NH_4^+ and NO_2^- concentrations (Table 1).

In fall at the Silex pond and in winter at both the Pêcheries and Silex ponds, there were clear sub-daily variations in %N_2O that were uncorrelated to %O_2 variations. %O_2 decreased during day-time, but %N_2O either showed erratic changes (the Silex pond in winter), a decreasing tendency (the Pêcheries pond in winter), or an increasing tendency (the Silex pond in fall). There was no clear explanation for these divergent patterns and why they differed from those described above for spring and summer.

The %O_2, pCO_2, CH_4, and %N_2O data collected at sub-daily scale from this study were within the range and the means were comparable to the seasonal data from Bauduin et al. (2024a) in the same ponds based on a dense seasonal sampling from June 2021 to December 2023 (once a day from one (winter) to three (summer) times per month) (Table S2).

3.2. Variations of CO_2, CH_4 and N_2O fluxes at sub-daily scale

The air-water diffusive CO_2 fluxes (F_{CO2}) at the Pêcheries pond for all sub-daily samplings ranged from 10 to 671 mmol m^{-2} d^{-1} in winter and in fall, respectively (Fig. S4). The amplitude of sub-daily variations of F_{CO2} at the Pêcheries pond was minimal in winter (14 mmol m^{-2} d^{-1}) and maximal in fall (496 mmol m^{-2} d^{-1}). The F_{CO2} fluxes at the Silex pond for all sub-daily samplings ranged from 50 to 467 mmol m^{-2} d^{-1} in summer and fall, respectively. The amplitude of sub-daily variation of F_{CO2} at the Silex pond was minimal in summer (39 mmol m^{-2} d^{-1}) and maximal in fall (274 mmol m^{-2} d^{-1}). The air-water diffusive CH_4 fluxes (F_{CH4}) at the Pêcheries pond for all sub-daily samplings ranged from 130 to 4847 µmol m^{-2} d^{-1} in winter and summer, respectively. The amplitude of sub-daily variation of F_{CH4} at the Pêcheries pond was minimal in winter (59 µmol m^{-2} d^{-1}) and maximal in fall (3076 µmol m^{-2} d^{-1}) (Fig. S4). The F_{CH4} at the Silex pond for all sub-daily samplings ranged from 348 to 9334 µmol m^{-2} d^{-1} in winter and summer, respectively. The amplitude of sub-daily variation of F_{CH4} at the Silex pond was minimal in winter (497 µmol m^{-2} d^{-1}) and maximal in summer (6291 µmol m^{-2} d^{-1}). The air-water diffusive N_2O fluxes (F_{N2O}) in the two ponds were sometimes positive (source of N_2O to the atmosphere) and sometimes negative (sink of atmospheric N_2O), given that %N_2O oscillated around saturation (100%) (Fig. 3, S4). The F_{N2O} at the Pêcheries pond for all sub-daily samplings ranged from −1.3 to 0.5 µmol m^{-2} d^{-1} in spring and summer, respectively. The amplitude of variation of F_{N2O} at the Pêcheries pond was minimal in winter (0.2 µmol m^{-2} d^{-1}) and maximal in spring (1.3 µmol m^{-2} d^{-1}) (Fig. S4). The F_{N2O} at the Silex pond for all sub-daily samplings ranged from −1.8 to 8.1 µmol m^{-2} d^{-1} in spring and fall, respectively. The amplitude of variation of F_{N2O} at the Silex pond was minimal in winter (0.8 µmol m^{-2} d^{-1}) and maximal in fall (3.9 µmol m^{-2} d^{-1}).

The F_{CO2}, F_{CH4}, and F_{N2O} were calculated from k with a parameterization as a function of wind speed (Cole and Caraco, 1998) and from the air-water gradient of the respective GHG concentration. Both wind speed and GHG concentrations can vary at daily scale leading potentially to differences in the intensity of flux during day-time and during night-time (Fig. 1). To investigate sources of sub-daily variability of F_{CO2}, F_{CH4}, and F_{N2O}, the data were averaged over 3 periods each day: end of the night and early morning; mid-morning to mid-afternoon, late after-noon and early night (Figs. S5 and S6).

At the Pêcheries pond, the wind speed was higher in the middle of the day in spring, summer and fall, and increased from late night to early night in winter (Fig. S5). The F_{CO2} at the Pêcheries pond were higher in the middle of the day than during the rest of the day in summer and fall, following the pattern of the wind speed. In spring, the F_{CO2} at the Pêcheries pond were higher at the start of the day and decreased over the course of the day, as pCO_2. In winter, the F_{CO2} at the Pêcheries pond increased throughout the day, as wind speed and pCO_2 (Fig. S5). The F_{CH4} at the Pêcheries pond followed concentration changes in spring, and wind speed changes in summer, fall and winter (Fig. S5).

At the Silex pond, wind speed was higher in the middle of the day in spring and fall (Fig. S5). In summer, the wind was higher at the beginning of the day than at the end, and in winter, the wind was nearly constant throughout the day, at the Silex pond (Fig. S5). The F_{CO2} at the Silex pond followed wind speed variations in each season. The F_{CH4} at the Silex pond followed wind speed variations in spring, fall and winter. In summer, the F_{CH4} at the Silex pond were highest in the middle of the day and followed the CH_4 concentrations (Fig. S5).

In both ponds, N_2O fluxes sometimes followed wind speed (winter at the Pêcheries pond), sometimes changes in concentrations (summer at the Pêcheries pond), sometimes wind speed and concentrations (fall at the Silex pond). In most cases, the sub-daily variations of F_{N2O} did not show clear patterns for the three periods of the day (Fig. S5).

3.3. Comparison of sub-daily variability to seasonal and spatial variability of GHG concentrations and fluxes

The coefficient of variation (CV, in %) was used to compare the sub-daily variability of the GHG concentrations and fluxes with the variability at seasonal scale within the same pond (hereafter “intra-pond”

CV) and the variability among several ponds in the city of Brussels (hereafter “inter-pond” CV). The intra-pond seasonal CV was estimated from a data-set acquired in the Pêcheries and Silex ponds with a sampling from one (winter) to three (summer) times per month in 2021, 2022 and 2023 (Bauduin et al., 2024a). The inter-pond CV was estimated from a data-set acquired in 22 ponds sampled only once per season, during the four seasons, in 2021–2022 (Bauduin et al., 2024b).

The sub-daily CV of pCO_2 ranged between 2 and 32% in the Pêcheries pond and between 0.9 and 4.5% in the Silex pond (Fig. 5). The highest sub-daily CV of pCO_2 (32%) was observed in the Pêcheries pond in spring presumably due to intense phytoplankton photosynthesis during the spring bloom. In both ponds, the sub-daily variability of pCO_2 was lower than the intra-pond seasonal CV (45–67% in the Pêcheries pond and 22–47% in the Silex pond) and the inter-pond CV (55–90%).

The sub-daily CV of CH_4 dissolved concentration ranged between 2 and 101% in the Pêcheries pond and between 4 and 33% in the Silex pond (Fig. 5). The highest sub-daily CV of CH_4 dissolved concentration (101%) was observed in the Pêcheries pond in summer presumably due to an ebullition event (see above). In both ponds, the sub-daily variability of CH_4 dissolved concentration was lower than the intra-pond seasonal CV (45–100% in the Pêcheries pond and 46–75% in the Silex pond) and the inter-pond CV (67–156%).

The sub-daily CV of $\%N_2O$ ranged between 1 and 13% in the Pêcheries pond and between 2 and 7% in the Silex pond (Fig. 5). In both ponds, the sub-daily variability of $\%N_2O$ was lower than the intra-pond seasonal CV (22–35% in the Pêcheries pond and 19–74% in the Silex pond) and the inter-pond CV (52–332%).

The sub-daily, intra-pond seasonal, and inter-pond variability (CV) of diffusive F_{CO2} and F_{CH4} showed the same patterns and were numerically close to those of pCO_2 and CH_4 dissolved concentration (Figs. 5 and 6). The sub-daily CV of F_{N2O} ranged between 28 and 189% in the Pêcheries pond and between 21 and 58% in the Silex pond (Fig. 6), and was substantially higher than the respective CV of $\%N_2O$ (Fig. 6). In both ponds, the sub-daily variability of F_{N2O} was lower than the intra-pond seasonal CV (74–1492% in the Pêcheries pond and 150–252% in the Silex pond) and the inter-pond CV (115–389%). The studied ponds oscillated seasonally and among different ponds between a sink and source of N_2O (Bauduin et al. 2024a, 2024b), so the average was close to zero, leading to a numerical increase of CV of F_{N2O} compared to the respective CV of $\%N_2O$. The CV of F_{CO2}, F_{CH4}, and F_{N2O} computed with a k derived from a constant average wind speed (1 m s^{-1}) (Fig. S7) exhibited similar patterns and were numerically comparable to those calculated using actual wind speed data (Fig. 6). This showed that the variability (CV) of F_{CO2}, F_{CH4}, and F_{N2O} was mainly driven by changes in CO_2, CH_4, and N_2O concentrations rather than changes in computed k from a parameterization function of wind speed. Indeed, in the studied ponds, variations of wind speed are modest at sub-daily (Fig. S1) and seasonal (Bauduin et al. 2024a, 2024b) scales.

For the three GHGs, whether concentrations or fluxes, the variability (CV) tended to be higher in spring-summer than fall-winter at all scales

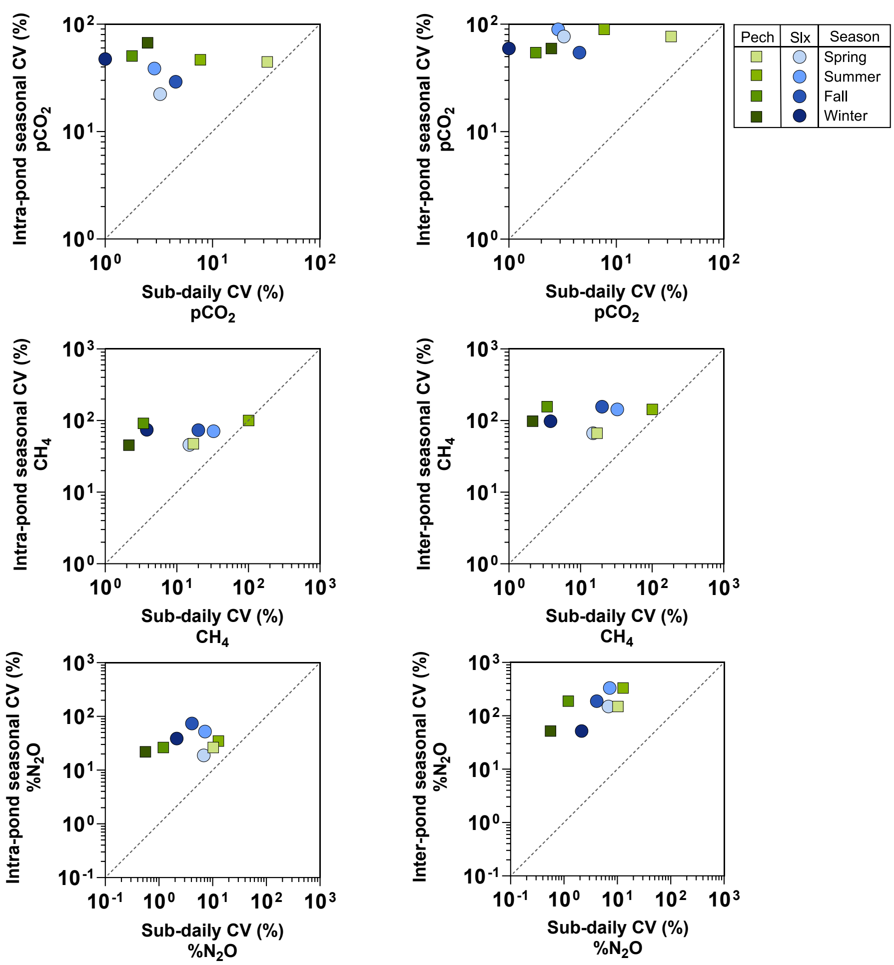

Fig. 5. Coefficients of variation of data collected from June 2021 to December 2023 at Pêcheries (Pech) and Silex (Slx) ponds (intra-pond seasonal CV, in %) from Bauduin et al. (2024a) and coefficients of variation of data collected on 22 ponds in Brussels at the four seasons in 2021 and 2022 (inter-pond seasonal CV, in %) from Bauduin et al. (2024b) versus coefficients of variation of sub-daily data at the Pêcheries and Silex ponds from this study (sub-daily CV, in %) for partial pressure of CO_2 (pCO_2, in ppm), dissolved CH_4 concentration (CH_4, in nmol L^{-1}), and N_2O saturation level ($\%N_2O$, in %). Dotted line indicates the 1:1 line.

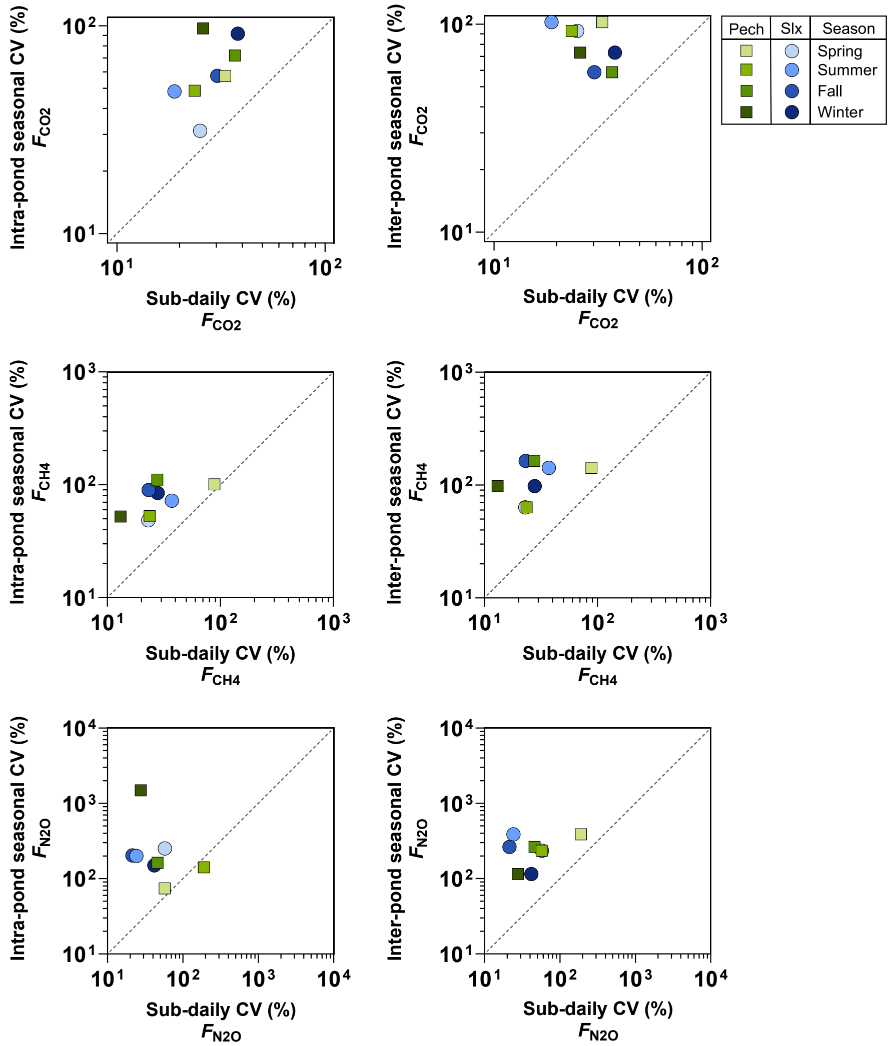

Fig. 6. Coefficients of variation of data collected from June 2021 to December 2023 at Pêcheries (Pech) and Silex (Slx) ponds (intra-pond seasonal CV, in %) from Bauduin et al. (2024a) and coefficient of variation of data collected on 22 ponds in Brussels at the four seasons in 2021 and 2022 (inter-pond seasonal CV, in %) from Bauduin et al. (2024b) versus coefficients of variation of sub-daily data at the Pêcheries and Silex ponds from this study (sub-daily CV, in %) for diffusive fluxes of CO_2 (F_{CO2}, in mmol m^{-2} d^{-1}), CH_4 (F_{CH4}, in µmol m^{-2} d^{-1}) and N_2O (F_{N2O}, in µmol m^{-2} d^{-1}), computed from hourly wind speed measurements; Fig. S7 reports F_{CO2}, F_{CH4}, and F_{N2O} computed with a constant wind speed of 1 m s^{-1}. Dotted line indicates the 1:1 line.

(sub-daily, seasonal intra-pond, and inter-pond). Indeed, the CV of the GHG concentrations was in most cases positively related to water temperature (Fig. S8), although less clear for fluxes due to the additional variability from wind speed (Fig. S9). In spring and summer, higher temperatures increase all aquatic metabolic processes, and, in addition, higher primary production in response to better light conditions directly affects CO_2 levels and cascades to enhance microbial processes that also affect CO_2 (respiration), as well as CH_4 (methanogenesis), and N_2O (nitrification and denitrification).

3.4. Comparison of GHG sub-daily variations with other lakes and ponds

There is only a limited number of equivalent studies of the sub-daily variability of CO_2, CH_4, and N_2O emissions from lakes and ponds (Zhang et al., 2018, 2023; Xiao et al., 2019; Martinez-Cruz et al., 2020; Sieczko et al., 2020; Rudberg et al., 2021; Borges et al., 2022; Ni et al., 2022; Sø et al., 2023, 2024; Shen et al., 2024; Smith et al., 2024; Wang et al., 2024a, 2024b), and, none reporting simultaneous measurements of the three GHGs. In general, previous studies showed that during periods of active aquatic primary production, the CO_2 concentration followed the light cycle with decreasing values during day-time and increasing values during night-time, in response to cycles of photosynthesis and respiration (Borges et al., 2022; Wang et al., 2024a, 2024b; Shen et al., 2024). The actual net F_{CO2} also depended on wind speed that was generally higher during day-time (Martinez-Cruz et al., 2020; Rudberg et al., 2021; Borges et al., 2022; Sø et al., 2023, 2024). These patterns of CO_2 dissolved concentrations and computed F_{CO2} were also observed in spring and summer in the Silex and the Pêcheries ponds (Fig. 3, S4). During fall and winter, when aquatic primary production was putatively lower owing to lower temperature and light availability (Table 1), the patterns of CO_2 dissolved concentrations and computed F_{CO2} were more erratic and with lower amplitude in the Silex and the Pêcheries ponds (Fig. 3, S4).

In general, previous studies showed that the higher wind speeds during day-time seemed to systematically lead to higher F_{CH4} from lakes and ponds during day-time (Zhang et al., 2018, 2023; Martinez-Cruz et al., 2020; Sieczko et al., 2020; Sø et al., 2023, 2024). In the Pêcheries and the Silex ponds, in nearly all the occasions, the sub-daily variations of F_{CH4} followed those of wind speed that frequently peaked in the middle of the day (Figs. S5 and S6). However, nearly all of the reported studies on diel variations of F_{CH4} from lakes and ponds were based on floating chambers (Zhang et al., 2018, 2023; Sieczko et al., 2020; Sø et al., 2023, 2024). Floating chambers provide the net F_{CH4} but do not allow discriminating the individual contribution to the observed variability of F_{CH4} from changes in CH_4 dissolved concentration and from those of *k*, with the additional complication that floating chambers can potentially also capture the ebullitive component of F_{CH4}. There are theoretical grounds for hypothesizing variations of CH_4 dissolved concentrations at sub-daily scale in surface waters of ponds and lakes summarized in Fig. 1, but they do not seem discernible in observational studies available so far. Zhang et al. (2018) observed erratic sub-daily variations of CH_4 dissolved concentration in an urban sub-tropical pond in the city of Yichang (Central China). In the Pêcheries and the Silex ponds, the variations of CH_4 dissolved concentrations were also mostly erratic in fall and winter or inconsistent among ponds in spring and summer (Fig. 4). If such a lack of consistent night-day variations in CH_4 dissolved concentrations is ubiquitous, it would suggest the prevalence of the variability of wind speed in driving sub-daily variations of F_{CH4} from lakes and ponds.

In nearly all occasions, N_2O dissolved concentrations showed erratic variations at sub-daily scale in the Pêcheries and the Silex ponds (Fig. 4) as also observed in Lake Taihu (China) (Xiao et al., 2019) and in Ashumet pond (U.S.A.) (Smith et al., 2024). On a limited number of occasions in the Pêcheries pond (spring and summer) and the Silex pond (spring), the N_2O dissolved levels peaked with the O_2 dissolved concentration, as also reported by Ni et al. (2022) in Lake Wuliangsuhai (China). However, an unequivocal explanation could not be provided for this pattern. On another limited number of occasions in the Silex pond (summer and fall), the N_2O levels were negatively correlated to O_2 dissolved concentration. Although such a pattern has not been reported at sub-daily scales in lakes and ponds, a night-time increase of N_2O in parallel to the lowering of O_2 in the water column has been frequently reported in rivers (Harrison et al., 2005; Clough et al., 2007; Baulch et al., 2012; Xia et al., 2013; Chen et al., 2021).

4. Conclusions

Data of pCO_2, CH_4 concentration, and $\%N_2O$ were collected hourly in two equally shallow (depth ~1m) and small (surface area ~1ha) urban ponds in the city of Brussels, the Pêcheries pond dominated by phytoplankton and the Silex pond dominated by macrophytes, during each of the four seasons in 2023–2024, with the aim to investigate if diurnal variations in the concentrations and fluxes of CO_2, CH_4, and N_2O in the two ponds were detectable, systematic, and could be explained mechanistically by biogeochemical drivers or meteorological conditions.

pCO_2 and $\%O_2$ followed expected temporal patterns from dawn to dusk in response to photosynthetic activity in the Pêcheries and the Silex ponds in spring and summer, as well as in fall at the Pêcheries pond. In winter, pCO_2 sub-daily variations were erratic in both ponds. The patterns of temporal changes from dawn to dusk of CH_4 dissolved concentration and $\%N_2O$ were more variable, were not systematically consistent during the different sampling periods and among the two ponds, and were more difficult to interpret than those of CO_2. Some of the temporal patterns of CH_4 dissolved concentration and $\%N_2O$ could be interpreted as resulting from the effect of an increase during day-time of O_2 diffusion from the water column to the sediments, and the resulting effect on sediment biogeochemical processes (MOX and nitrification, respectively). Some temporal patterns fitted with alternate explanations such as light inhibition of MOX leading to an increase of CH_4 during day-time or production of N_2O by microalgae themselves leading to an increase of $\%N_2O$ during day-time.

The sub-daily variations of F_{CO2} and F_{CH4} were in most cases dominated by the variations of wind speed that was frequently but not systematically higher during the middle of the day compared to early morning or late afternoon. In other cases, the sub-daily variations of F_{CO2} and F_{CH4} were dominated by the variations of GHG concentrations when their amplitude was more important and/or when the wind speed was relatively invariant. The sub-daily variations of F_{N2O} were mostly erratic whatever the pond and season.

The major limitation of the present work arose from the manual sampling leading to limited time-series with a high demand in human-power. The automation of measurements of dissolved concentrations with moored detectors of GHG dissolved concentrations (e.g. Hunt et al., 2017; Wang et al., 2024a,b) or of air-water GHG fluxes with automated floating chambers (e.g. Sieczko et al., 2020; Rudberg et al., 2021; Sø et al., 2023, 2024) should allow to provide more extensive time series. More extensive time series of GHG dissolved concentrations and/or fluxes should allow to better understand the drivers of daily variations of CO_2 and CH_4 emissions from ponds and lakes, however, technology to make equivalent instrumentation is at the moment lacking for N_2O.

The sub-daily variability, quantified by the CV, in the two ponds during the four seasons was lower for pCO_2 (CV<10% except one occasion), highest for CH_4 dissolved concentration (CV<50% except one occasion), and intermediary for $\%N_2O$ (CV<20%). The sub-daily variability of the three GHG concentrations tended to be more important in spring-summer than fall-winter. In both ponds, the sub-daily variability of the concentrations of the three GHGs was lower than the seasonal variability within individual ponds (CV>20%). In both ponds, the sub-daily variability of the concentrations of the three GHGs was also lower than the variability among 22 ponds in the city of Brussels (CV>50%). The same patterns of CV were observed for F_{CO2}, F_{CH4}, and F_{N2O} than for their respective concentrations, although the CV of the fluxes of N_2O was higher than for $\%N_2O$. The studied ponds oscillated seasonally and among different ponds between a sink and source of N_2O, so the average was close to zero, leading to a numerical increase of CV, unlike CO_2 and CH_4 that were systematically distinctly above saturation.

It is concluded that the variability of CO_2, CH_4, and N_2O concentrations and fluxes either seasonally within a given system or among different ponds seemed more important than the variability at sub-daily scales. This implies that to reduce the uncertainty on the estimate of CO_2, CH_4, and N_2O emissions from urban ponds a priority should be given to describe inter-system variability, followed by seasonal variability, and then sub-daily variability. Furthermore, the very strong dominance of sub-daily variations of wind speed in driving the diel variability of GHG emissions rather than the sub-daily variations of the dissolved concentrations of GHGs, allows concluding that the timing of the day for a spot concentration measurement when continuous measurements are not possible is of marginal importance. The bias in the computation of the flux can be reduced by correctly accounting for sub-daily variability in wind speed, especially for CH_4 and N_2O for which sub-daily variability of dissolved concentrations seemed mostly erratic. Both these conclusions can be used to inform when designing sampling strategies and optimizing the allocation of available resources for a systematic quantification of GHG emissions from water bodies in the context of the environmental management of inland waters, including urban ponds.

CRediT authorship contribution statement

Thomas Bauduin: Writing – original draft, Visualization, Investigation, Formal analysis, Data curation, Conceptualization. **Nathalie Gypens:** Writing – original draft, Validation, Supervision, Resources, Project administration, Methodology, Funding acquisition, Formal analysis. **Alberto V. Borges:** Writing – original draft, Visualization, Supervision, Resources, Project administration, Methodology, Funding acquisition, Formal analysis, Data curation, Conceptualization.

Funding

TB received funding from Institute for the Encouragement of Scientific Research and Innovation (Innoviris) of the Brussels-Capital Region as part of the Smartwater project (RBC/2020-EPF-6 h) and from the

"Fonds pour la formation à la Recherche dans l'Industrie et dans l'Agriculture" (FRIA, Belgium). The Picarro G2201-i isotopic analyzer was funded by FRS-FNRS (U.N005.21).

Declaration of competing interest

The authors declare that they have no known competing financial interests or personal relationships that could have appeared to influence the work reported in this paper.

Acknowledgements

Ozan Efe (University of Liège) analysed CH_4/N_2O concentrations and $\delta^{13}C$-CH_4, Cédric Morana (University of Liège) helped setting up the Picarro G2201-*i* isotopic analyzer, Brussels Environment provided data on pond morphology, five anonymous reviewers provided comments that allowed to improve the original manuscript. AVB is a Research Director at the FRS-FNRS.

Appendix A. Supplementary data

Supplementary data to this article can be found online at https://doi.org/10.1016/j.jenvman.2024.123627.

Data availability

The data supporting this study are available at https://zenodo.org/records/11395489.

References

American Public Health Association (APHA), 1998. Standard Methods for the Examination of Water and Wastewater, sixth ed. American Public Health Association.

Bauduin, T., Gypens, N., Borges, A.V., 2024a. Methane, carbon dioxide and nitrous oxide emissions from two clear-water and two turbid-water urban ponds in Brussels (Belgium). Biogeosciences Discussion 1–29. https://doi.org/10.5194/egusphere-2024-1315.

Bauduin, T., Gypens, N., Borges, A.V., 2024b. Seasonal and spatial variations of greenhouse gas (CO_2, CH_4 and N_2O) emissions from urban ponds in Brussels. Water Res. 253, 1–14. https://doi.org/10.1016/j.watres.2024.121257.

Baulch, H.M., Dillon, P.J., Maranger, R., Venkiteswaran, J.J., Wilson, H.F., Schiff, S.L., 2012. Night and day: short-term variation in nitrogen chemistry and nitrous oxide emissions from streams. Freshw. Biol. 57, 509–525. https://doi.org/10.1111/j.1365-2427.2011.02720.x.

Bižić, M., Klintzsch, T., Ionescu, D., Hindiyeh, M.Y., Günthel, M., Muro-Pastor, A.M., Eckert, W., Keppler, F., Grossart, H.P., 2020. Aquatic and terrestrial cyanobacteria produce methane. Sci. Adv. 6, 1–9. https://doi.org/10.1126/sciadv.aax5343.

Borges, A.V., Darchambeau, F., Lambert, T., Morana, C., Allen, G.H., Tambwe, E., Sembaito, A.T., Mambo, T., Wabakhangazi, J.N., Descy, J.-P., Teodoru, C., Bouillon, S., 2019. Variations in dissolved greenhouse gases (CO_2, CH_4, N_2O) in the Congo River network overwhelmingly driven by fluvial-wetland connectivity. Biogeosciences 16, 3801–3834. https://doi.org/10.5194/bg-16-3801-2019.

Borges, A.V., Darchambeau, F., Lambert, T., Bouillon, S., Morana, C., Brouyère, S., Hakoun, V., Jurado, A., Tseng, H.-C., Descy, J.-P., Roland, F.A.E., 2018. Effects of agricultural land use on fluvial carbon dioxide, methane and nitrous oxide concentrations in a large European river, the Meuse (Belgium). Sci. Total Environ. 610–611, 342–355. https://doi.org/10.1016/j.scitotenv.2017.08.047.

Borges, A.V., Deirmendjian, L., Bouillon, S., Okello, W., Lambert, T., Roland, F.A.E., Razanamahandry, V.F., Voarintsoa, N.R.G., Darchambeau, F., Kimirei, I.A., Descy, J., Allen, G.H., Morana, C., 2022. Greenhouse gas emissions from African lakes are no longer a blind spot. Sci. Adv. 8, 1–17. https://doi.org/10.1126/sciadv.abi8716.

Borges, A.V., Okello, W., Bouillon, S., Deirmendjian, L., Nankabirwa, A., Nabafu, E., Lambert, T., Descy, J.-P., Morana, C., 2023. Spatial and temporal variations of dissolved CO2, CH4 and N2O in lakes edward and george (east africa). J. Great Lake. Res. 49, 229–245. https://doi.org/10.1016/j.jglr.2022.11.010.

Burlacot, A., Richaud, P., Gosset, A., Li-Beisson, Y., Peltier, G., 2020. Algal photosynthesis converts nitric oxide into nitrous oxide. Proc. Natl. Acad. Sci. USA 117, 2704–2709. https://doi.org/10.1073/pnas.1915276117.

Cael, B.B., Heathcote, A.J., Seekell, D.A., 2017. The volume and mean depth of Earth's lakes. Geophys. Res. Lett. 44, 209–218. https://doi.org/10.1002/2016GL071378.

Casas-Ruiz, J.P., Hutchins, R.H., del Giorgio, P.A., 2021a. Total aquatic carbon emissions across the boreal biome of Québec driven by watershed slope. J. Geophys. Res.: Biogeosciences 126, 1–18. https://doi.org/10.1029/2020JG005863.

Casas-Ruiz, J.P., Jakobsson, J., del Giorgio, P.A., 2021b. The role of lake morphometry in modulating surface water carbon concentrations in boreal lakes. Environ. Res. Lett. 16, 1–11. https://doi.org/10.1088/1748-9326/ac0be3.

Chen, X., Wang, K., Li, X., Qiao, Y., Dong, K., Yang, L., 2021. Microcystis blooms aggravate the diurnal alternation of nitrification and nitrate reduction in the water column in Lake Taihu. Sci. Total Environ. 767, 1–9. https://doi.org/10.1016/j.scitotenv.2020.144884.

Clough, T.J., Buckthought, L.E., Kelliher, F.M., Sherlock, R.R., 2007. Diurnal fluctuations of dissolved nitrous oxide (N_2O) concentrations and estimates of N_2O emissions from a spring-fed river: implications for IPCC methodology. Global Change Biol. 13, 1016–1027. https://doi.org/10.1111/j.1365-2486.2007.01337.x.

Cole, J.J., Caraco, N.F., 1998. Atmospheric exchange of carbon dioxide in a low-wind oligotrophic lake measured by the addition of SF6. Limnol. Oceanogr. 43, 647–656. https://doi.org/10.4319/lo.1998.43.4.0647.

De Backer, S., Van Onsem, S., Triest, L., 2010. Influence of submerged vegetation and fish abundance on water clarity in peri-urban eutrophic ponds. Hydrobiologia 656, 255–267. https://doi.org/10.1007/s10750-010-0444-z.

Deemer, B.R., Holgerson, M.A., 2021. Drivers of methane flux differ between lakes and reservoirs, complicating global upscaling efforts. J. Geophys. Res.: Biogeosciences 126, 1–15. https://doi.org/10.1029/2019JG005600.

DelSontro, T., Beaulieu, J.J., Downing, J.A., 2018. Greenhouse gas emissions from lakes and impoundments: upscaling in the face of global change. Limnology and Oceanography Letters 3, 64–75. https://doi.org/10.1002/lol2.10073.

Dumestre, J.F., Guézennec, J., Galy-Lacaux, C., Delmas, R., Richard, S., Labroue, L., 1999. Influence of light intensity on methanotrophic bacterial activity in Petit Saut Reservoir, French Guiana. Appl. Environ. Microbiol. 65, 534–539. https://doi.org/10.1128/AEM.65.2.534-539.1999.

Dutton, G., Elkins II, J., Hall, B., 2017. NOAA ESRL, Earth System Research Laboratory Halocarbons and Other Atmospheric Trace Gases Chromatograph for Atmospheric Trace Species (CATS) Measurements. NOAA National Centers for Environmental Information. https://doi.org/10.7289/V5X0659V.

Erkkilä, K.M., Ojala, A., Bastviken, D., Biermann, T., Heiskanen, J.J., Lindroth, A., Peltola, O., Rantakari, M., Vesala, T., Mammarella, I., 2018. Methane and carbon dioxide fluxes over a lake: comparison between eddy covariance, floating chambers and boundary layer method. Biogeosciences 15, 429–445. https://doi.org/10.5194/bg-15-429-2018.

Fabisik, F., Guieysse, B., Procter, J., Plouviez, M., 2023. Nitrous oxide (N_2O) synthesis by the freshwater cyanobacterium Microcystis aeruginosa. Biogeosciences 20, 687–693. https://doi.org/10.5194/bg-20-687-2023.

Franz, D., Koebsch, F., Larmanou, E., Augustin, J., Sachs, T., 2016. High net CO_2 and CH_4 release at a eutrophic shallow lake on a formerly drained fen. Biogeosciences 13, 3051–3070. https://doi.org/10.5194/bg-13-3051-2016.

Golub, M., Koupaei-Abyazani, N., Vesala, T., Mammarella, I., Ojala, A., Bohrer, G., Weyhenmeyer, G.A., Blanken, P.D., Eugster, W., Koebsch, F., Chen, J., Czajkowski, K., Deshmukh, C., Guérin, F., Heiskanen, J., Humphreys, E., Jonsson, A., Karlsson, J., Kling, G., Lee, X., Liu, H., Lohila, A., Lundin, E., Morin, T., Podgrajsek, E., Provenzale, M., Rutgersson, A., Sachs, T., Sahlée, E., Serça, D., Shao, C., Spence, C., Strachan, I.B., Xiao, W., Desai, A.R., 2023. Diel, seasonal, and inter-annual variation in carbon dioxide effluxes from lakes and reservoirs. Environ. Res. Lett. 18, 1–14. https://doi.org/10.1088/1748-9326/acb834.

Goreau, T.J., Kaplan, W.A., Wofsy, S.C., McElroy, M.B., Valois, F.W., Watson, S.W., 1980. Production of NO_2-and N_2O by nitrifying bacteria at reduced concentrations of oxygen. Appl. Environ. Microbiol. 40, 526–532. https://doi.org/10.1128/aem.40.3.526-532.1980.

Grasshoff, K., Johannsen, H., 1972. A new sensitive and direct method for the automatic determination of ammonia in sea water. ICES (Int. Counc. Explor. Sea) J. Mar. Sci. 34, 516–521. https://doi.org/10.1093/icesjms/34.3.516.

Grasshoff, K., Kremling, K., Ehrhardt, M., 2009. Methods of Seawater Analysis: Determination of Nitrite, 10.2. John Wiley & Sons, pp. 177–180.

Guérin, F., Abril, G., Serça, D., Delon, C., Richard, S., Delmas, R., Tremblay, A., Varfalvy, L., 2007. Gas transfer velocities of CO_2 and CH_4 in a tropical reservoir and its river downstream. J. Mar. Syst. 66, 161–172. https://doi.org/10.1016/j.jmarsys.2006.03.019.

Guieysse, B., Plouviez, M., Coilhac, M., Cazali, L., 2013. Nitrous Oxide (N_2O) production in axenic Chlorella vulgaris microalgae cultures: evidence, putative pathways, and potential environmental impacts. Biogeosciences 10, 6737–6746. https://doi.org/10.5194/bg-10-6737-2013.

Harrison, J.A., Matson, P.A., Fendorf, S.E., 2005. Effects of a diel oxygen cycle on nitrogen transformations and greenhouse gas emissions in a eutrophied subtropical stream. Aquat. Sci. 67, 308–315. https://doi.org/10.1007/s00027-005-0776-3.

Hofmann, H., Federwisch, L., Peeters, F., 2010. Wave-induced release of methane: littoral zones as source of methane in lakes. Limnol. Oceanogr. 55, 1990–2000. https://doi.org/10.4319/lo.2010.55.5.1990.

Holgerson, M.A., Raymond, P.A., 2016. Large contribution to inland water CO_2 and CH_4 emissions from very small ponds. Nat. Geosci. 9, 222–226. https://doi.org/10.1038/ngeo2654.

Holgerson, M.A., Farr, E.R., Raymond, P.A., 2017. Gas transfer velocities in small forested ponds. J. Geophys. Res.: Biogeosciences 122, 1011–1021. https://doi.org/10.1002/2016JG003734.

Hunt, C.W., Snyder, L., Salisbury, J.E., Vandemark, D., McDowell, W.H., 2017. SIPCO2: a simple, inexpensive surface water pCO2 sensor. Limnol Oceanogr. Methods 15, 291–301. https://doi.org/10.1002/lom3.10157.

Jammet, M., Dengel, S., Kettner, E., Parmentier, F.J.W., Wik, M., Crill, P., Friborg, T., 2017. Year-round CH_4 and CO_2 flux dynamics in two contrasting freshwater ecosystems of the subarctic. Biogeosciences 14, 5189–5216. https://doi.org/10.5194/bg-14-5189-2017.

Klaus, M., Vachon, D., 2020. Challenges of predicting gas transfer velocity from wind measurements over global lakes. Aquat. Sci. 82, 1–17. https://doi.org/10.1007/s00027-020-00729-9.

Koroleff, J., 1983. Determination of total phosphorus by alkaline persulphate oxidation. Methods of Seawater Analysis. Verlag Chemie, Wienheim, pp. 136–138.
Lan, X., Thoning, K.W., Dlugokencky, E.J., 2024. Trends in globally-averaged CH_4, N_2O, and SF_6 determined from NOAA global monitoring laboratory measurements. Version 2024-10. https://doi.org/10.15138/P8XG-AA10.
Lauerwald, R., Allen, G.H., Deemer, B.R., Liu, S., Maavara, T., Raymond, P., Alcott, L., Bastviken, D., Hastie, A., Holgerson, M.A., Johnson, M.S., Lehner, B., Lin, P., Marzadri, A., Ran, L., Tian, H., Yang, X., Yao, Y., Regnier, P., 2023. Inland water greenhouse gas budgets for RECCAP2: 2. Regionalization and homogenization of estimates. Global Biogeochem. Cycles 37, 1–16. https://doi.org/10.1029/2022GB007658.
Lenhart, K., Behrendt, T., Greiner, S., Steinkamp, J., Well, R., Giesemann, A., Keppler, F., 2019. Nitrous oxide effluxes from plants as a potentially important source to the atmosphere. New Phytol. 221, 1398–1408. https://doi.org/10.1111/nph.15455.
Liikanen, A., Tanskanen, H., Murtoniemi, T., Martikainen, P.J., 2002. A laboratory microcosm for simultaneous gas and nutrient flux measurements in sediments. Boreal Environ. Res. 7, 151–160.
Lorke, A., Peeters, F., 2006. Toward a unified scaling relation for interfacial fluxes. J. Phys. Oceanogr. 36, 955–961. https://doi.org/10.1175/JPO2903.1.
Maberly, S.C., Barker, P.A., Stott, A.W., De Ville, M.M., 2013. Catchment productivity controls CO_2 emissions from lakes. Nat. Clim. Change 3, 391–394. https://doi.org/10.1038/nclimate1748.
MacIntyre, S., Amaral, J.H.F., Melack, J.M., 2021a. Enhanced turbulence in the upper mixed layer under light winds and heating: implications for gas fluxes. J. Geophys. Res.: Oceans 126, 1–36. https://doi.org/10.1029/2020JC017026.
MacIntyre, S., Bastviken, D., Arneborg, L., Crowe, A.T., Karlsson, J., Andersson, A., Gålfalk, M., Rutgersson, A., Podgrajsek, A., Melack, J.M., 2021b. Turbulence in a small boreal lake: consequences for air–water gas exchange. Limnol. Oceanogr. 66, 827–854. https://doi.org/10.1002/lno.11645.
MacIntyre, S., Jonsson, A., Jansson, M., Aberg, J., Turney, D.E., Miller, S.D., 2010. Buoyancy flux, turbulence, and the gas transfer coefficient in a stratified lake. Geophys. Res. Lett. 37, 1–5. https://doi.org/10.1029/2010GL044164.
MacIntyre, S., Sickman, J.O., Goldthwait, S.A., Kling, G.W., 2006. Physical pathways of nutrient supply in a small, ultraoligotrophic arctic lake during summer stratification. Limnol. Oceanogr. 51, 1107–1124. https://doi.org/10.4319/lo.2006.51.2.1107.
Martinez-Cruz, K., Sepulveda-Jauregui, A., Greene, S., Fuchs, A., Rodriguez, M., Pansch, N., Gonsiorczyk, T., Casper, P., 2020. Diel variation of CH_4 and CO_2 dynamics in two contrasting temperate lakes. Inland Waters 10, 333–347. https://doi.org/10.1080/20442041.2020.1728178.
McGinnis, D.F., Flury, S., Tang, K.W., Grossart, H.P., 2017. Porewater methane transport within the gas vesicles of diurnally migrating Chaoborus spp.: an energetic advantage. Sci. Rep. 7, 1–7. https://doi.org/10.1038/srep44478.
Mengis, M., Gächter, R., Wehrli, B., 1997. Sources and sinks of nitrous oxide (N_2O) in deep lakes. Biogeochemistry 38, 281–301. https://doi.org/10.1023/A:1005814020322.
Morana, C., Bouillon, S., Nolla-Ardèvol, V., Roland, F.A., Okello, W., Descy, J.P., Nankabirwa, A., Nabafu, E., Springael, D., Borges, A.V., 2020. Methane paradox in tropical lakes? Sedimentary fluxes rather than pelagic production in oxic conditions sustain methanotrophy and emissions to the atmosphere. Biogeosciences 17, 5209–5221. https://doi.org/10.5194/bg-17-5209-2020.
Murase, J., Sugimoto, A., 2005. Inhibitory effect of light on methane oxidation in the pelagic water column of a mesotrophic lake (Lake Biwa, Japan). Limnol. Oceanogr. 50, 1339–1343. https://doi.org/10.4319/lo.2005.50.4.1339.
Ni, B.J., Ruscalleda, M., Pellicer-Nacher, C., Smets, B.F., 2011. Modeling nitrous oxide production during biological nitrogen removal via nitrification and denitrification: extensions to the general ASM models. Environmental science & technology 45, 7768–7776. https://doi.org/10.1021/es201489n.
Ni, M., Liang, X., Hou, L., Li, W., He, C., 2022. Submerged macrophytes regulate diurnal nitrous oxide emissions from a shallow eutrophic lake: a case study of Lake Wuliangsuhai in the temperate arid region of China. Sci. Total Environ. 811, 1–12. https://doi.org/10.1016/j.scitotenv.2021.152451.
Oswald, K., Milucka, J., Brand, A., Littmann, S., Wehrli, B., Kuypers, M.M., Schubert, C. J., 2015. Light-dependent aerobic methane oxidation reduces methane emissions from seasonally stratified lakes. PLoS One 10, 1–22. https://doi.org/10.1371/journal.pone.0132574.
Peretyatko, A., Symoens, J.J., Triest, L., 2007. Impact of macrophytes on phytoplankton in eutrophic peri-urban ponds, implications for pond management and restoration. Belg. J. Bot. 83–99. https://www.jstor.org/stable/20794626.
Peretyatko, A., Teissier, S., De Backer, S., Triest, L., 2012. Biomanipulation of hypereutrophic ponds: when it works and why it fails. Environ. Monit. Assess. 184, 1517–1531. https://doi.org/10.1007/s10661-011-2057-z.
Plouviez, M., Guieysse, B., 2020. Nitrous oxide emissions during microalgae-based wastewater treatment: current state of the art and implication for greenhouse gases budgeting. Water Sci. Technol. 82, 1025–1030. https://doi.org/10.2166/wst.2020.304.
Plouviez, M., Shilton, A., Packer, M.A., Guieysse, B., 2019. Nitrous oxide emissions from microalgae: potential pathways and significance. J. Appl. Phycol. 31, 1–8. https://doi.org/10.1007/s10811-018-1531-1.
Plouviez, M., Wheeler, D., Shilton, A., Packer, M.A., McLenachan, P.A., Sanz-Luque, E., Ocaña-Calahorro, F., Fernández, E., Guieysse, B., 2017. The biosynthesis of nitrous oxide in the green alga Chlamydomonas reinhardtii. Plant J. 91, 45–56. https://doi.org/10.1111/tpj.13544.
Podgrajsek, E., Sahlée, E., Rutgersson, A., 2014. Diurnal cycle of lake methane flux. J. Geophys. Res.: Biogeosciences 119, 236–248. https://doi.org/10.1002/2013JG002327.
R Core Team, 2021. R: A Language and Environment for Statistical Computing. R Foundation for Statistical Computing, Vienna, Austria. https://www.R-project.org/.
Ray, N.E., Holgerson, M.A., 2023. High intra-seasonal variability in greenhouse gas emissions from temperate constructed ponds. Geophys. Res. Lett. 50, 1–10. https://doi.org/10.1029/2023GL104235.
Ray, N.E., Holgerson, M.A., Andersen, M.R., Bikše, J., Bortolotti, L.E., Futter, M., Kokorīte, I., Law, A., McDonald, C., Mesman, J.P., Peacock, M., Richardson, C., Arsenault, J., Bansal, S., Cawley, K., Kuhn, M., Shahabinia, R., Smufer, F., 2023. Spatial and temporal variability in summertime dissolved carbon dioxide and methane in temperate ponds and shallow lakes. Limnol. Oceanogr. 68, 1530–1545. https://doi.org/10.1002/lno.12362.
Rocher-Ros, G., Harms, T.K., Sponseller, R.A., Väisänen, M., Mörth, C.M., Giesler, R., 2021. Metabolism overrides photo-oxidation in CO_2 dynamics of Arctic permafrost streams. Limnol. Oceanogr. 66, 169–181. https://doi.org/10.1002/lno.11564.
Rosamond, M.S., Thuss, S.J., Schiff, S.L., 2012. Dependence of riverine nitrous oxide emissions on dissolved oxygen levels. Nat. Geosci. 5, 715–718. https://doi.org/10.1038/ngeo1556.
Rudberg, D., Duc, N.T., Schenk, J., Sieczko, A.K., Pajala, G., Sawakuchi, H.O., Verheijen, H.A., Melack, J.-M., MacIntyre, S., Karlsson, J., Bastviken, D., 2021. Diel variability of CO_2 emissions from northern lakes. J. Geophys. Res.: Biogeosciences 126, 1–16. https://doi.org/10.1029/2021JG006246.
Scheffer, M., Hosper, S.H., Meijer, M.L., Moss, B., Jeppesen, E., 1993. Alternative equilibria in shallow lakes. Trends Ecol. Evol. 8, 275–279. https://doi.org/10.1016/0169-5347(93)90254-M.
Shen, C., Qian, M., Song, Y., Chen, B., Yang, J., 2024. Surface pCO_2 and air-water CO_2 fluxes dominated by submerged aquatic vegetation: implications for carbon flux in shallow lakes. J. Environ. Manag. 370, 1–10. https://doi.org/10.1016/j.jenvman.2024.
Sieczko, A.K., Duc, N.T., Schenk, J., Pajala, G., Rudberg, D., Sawakuchi, H.O., Bastviken, D., 2020. Diel Variability of Methane Emissions from Lakes, vol. 117. Proceedings of the National Academy of Sciences, pp. 21488–21494. https://doi.org/10.1073/pnas.2006024117.
Smith, R.L., Repert, D.A., Underwood, J.C., Böhlke, J.K., LeBlanc, D.R., Hull, R.B., Kent, D.B., Reed, A.P., Mroczkowski, S.J., 2024. Spatial, seasonal, and diel controls of nitrogen-carbon-oxygen cycling during lake-water infiltration to an aquifer. J. Geophys. Res.: Biogeosciences 129, 1–25. https://doi.org/10.1029/2023JG007659.
Sø, J.S., Martinsen, K.T., Kragh, T., Sand-Jensen, K., 2024. Hourly methane and carbon dioxide fluxes from temperate ponds. Biogeochemistry 167, 177–195. https://doi.org/10.1007/s10533-024-01124-4.
Sø, J.S., Sand-Jensen, K., Martinsen, K.T., Polauke, E., Kjær, J.E., Reitzel, K., Kragh, T., 2023. Methane and carbon dioxide fluxes at high spatiotemporal resolution from a small temperate lake. Sci. Total Environ. 878, 1–11. https://doi.org/10.1016/j.scitotenv.2023.162895.
Sollberger, S., Wehrli, B., Schubert, C.J., DelSontro, T., Eugster, W., 2017. Minor methane emissions from an Alpine hydropower reservoir based on monitoring of diel and seasonal variability. Environmental Science: Process. Impacts 19, 1278–1291. https://doi.org/10.1039/C7EM00232G.
Staehr, P.A., Christensen, J.P., Batt, R.D., Read, J.S., 2012. Ecosystem metabolism in a stratified lake. Limnol. Oceanogr. 57, 1317–1330. https://doi.org/10.4319/lo.2012.57.5.1317.
UNESCO/IHA, 2010. GHG Measurement Guidelines for Freshwater Reservoirs, UNESCO, vol. 138. The International Hydropower Association (IHA), London, UK. https://www.hydropower.org/publications/ghg-measurement-guidelines-for-freshwater-reservoirs.
Van Onsem, S., De Backer, S., Triest, L., 2010. Microhabitat–zooplankton relationship in extensive macrophyte vegetations of eutrophic clear-water ponds. Hydrobiologia 656, 67–81. https://doi.org/10.1007/s10750-010-0442-1.
Verpoorter, C., Kutser, T., Seekell, D.A., Tranvik, L.J., 2014. A global inventory of lakes based on high-resolution satellite imagery. Geophys. Res. Lett. 41, 6396–6402. https://doi.org/10.1002/2014GL060641.
Wang, Y., Ma, B., Shen, S., Zhang, Y., Ye, C., Jiang, H., Li, S., 2024a. Diel variability of carbon dioxide concentrations and emissions in a largest urban lake, Central China: insights from continuous measurements. Sci. Total Environ. 912, 1–12. https://doi.org/10.1016/j.scitotenv.2023.168987.
Wang, Y., Ma, B., Xu, Y.J., Shen, S., Huang, X., Wang, Y., Ye, S., Tian, X., Zhang, Y., Wang, T., Li, S., 2024b. Eutrophication and dissolved organic matter exacerbate the diel discrepancy of CO_2 emissions in China's largest urban lake. Environmental Science & Technology 1–11. https://doi.org/10.1021/acs.est.4c06244.
Wanninkhof, R., 1992. Relationship between wind speed and gas exchange over the ocean. J. Geophys. Res.: Oceans 97, 7373–7382. https://doi.org/10.1029/92JC00188.
Weathers, P.J., 1984. N_2O evolution by green algae. Appl. Environ. Microbiol. 48, 1251–1253. https://doi.org/10.1128/aem.48.6.1251-1253.1984.
Weiss, R.F., 1974. Carbon dioxide in water and seawater: the solubility of a non-ideal gas. Mar. Chem. 2, 203–215. https://doi.org/10.1016/0304-4203(74)90015-2.
Weiss, R.F., 1981. Determinations of carbon dioxide and methane by dual catalyst flame ionization chromatography and nitrous oxide by electron capture chromatography. Journal of Chromatographic Science 19, 611–616. https://doi.org/10.1093/chromsci/19.12.611.
Weiss, R.F., Price, B.A., 1980. Nitrous oxide solubility in water and seawater. Mar. Chem. 8, 347–359. https://doi.org/10.1016/0304-4203(80)90024-9.
Weyhenmeyer, G.A., Kosten, S., Wallin, M.B., Tranvik, L.J., Jeppesen, E., Roland, F., 2015. Significant fraction of CO_2 emissions from boreal lakes derived from hydrologic inorganic carbon inputs. Nat. Geosci. 8, 933–936. https://doi.org/10.1038/ngeo2582.

Wilson, S.T., Bange, H.W., Arévalo-Martínez, D.L., Barnes, J., Borges, A.V., Brown, I., Bullister, J.L., Burgos, M., Capelle, D.W., Casso, M., de la Paz, M., Farías, L., Fenwick, L., Ferrón, S., Garcia, G., Glockzin, M., Karl, D.M., Kock, A., Laperriere, S., Law, C.S., Manning, C.C., Marriner, A., Myllykangas, J.-K., Pholman, J.W., Rees, A.P., Santoro, A.E., Tortell, P.D., Upstill-Goddard, R.C., Wisegarver, D.P., Zhang, G.-L., Rehder, G., 2018. An intercomparison of oceanic methane and nitrous oxide measurements. Biogeosciences 15, 5891–5907. https://doi.org/10.5194/bg-15-5891-2018.

Xia, Y., Li, Y., Li, X., Guo, M., She, D., Yan, X., 2013. Diurnal pattern in nitrous oxide emissions from a sewage-enriched river. Chemosphere 92, 421–428. https://doi.org/10.1016/j.chemosphere.2013.01.038.

Xiao QiTao, X.Q., Zhang Mi, Z.M., Hu ZhengHua, H.Z., Gao YunQiu, G.Y., Hu Cheng, H.C., Liu Cheng, L.C., Shoudong, L., Shen, Z., JiaYu, Z., Wei, X., Lee, X., 2017. Spatial variations of methane emission in a large shallow eutrophic lake in subtropical climate. J. Geophys. Res.: Biogeosciences 122, 1597–1614. https://doi.org/10.1002/2017JG003805.

Xiao, Q., Xu, X., Qi, T., Luo, J., Lee, X., Duan, H., 2024. Lakes shifted from a carbon dioxide source to a sink over past two decades in China. Science bulletin 69, 1857–1861. https://doi.org/10.1016/j.scib.2024.03.022.

Xiao, Q., Xu, X., Zhang, M., Duan, H., Hu, Z., Wang, W., Xiao, W., Lee, X., 2019. Coregulation of nitrous oxide emissions by nitrogen and temperature in China's third largest freshwater lake (Lake Taihu). Limnol. Oceanogr. 64, 1070–1086. https://doi.org/10.1002/lno.11098.

Yamamoto, S., Alcauskas, J.B., Crozier, T.E., 1976. Solubility of methane in distilled water and seawater. J. Chem. Eng. Data 21, 78–80. https://doi.org/10.1021/je60068a029.

Yentsch, C.S., Menzel, D.W., 1963. A method for the determination of phytoplankton chlorophyll and phaeophytin by fluorescence. Deep Sea Research and Oceanographic Abstracts 10, 221–231. https://doi.org/10.1016/0011-7471(63)90358-9. Elsevier.

Zhang, C., Cheng, S., Long, L., Xie, H., Mu, X., Zhang, W., 2018. Diel and seasonal methane flux across water–air interface of a subtropic eutrophic pond. Toxicol. Environ. Chem. 100, 413–424. https://doi.org/10.1080/02772248.2018.1499231.

Zhang, Z., Li, J., Yu, R., Xia, X., Sun, H., Lu, C., Lu, X., 2023. Significant monthly and diel variations of CH_4 emission from a shallow eutrophic lake with submerged aquatic vegetation. Aquat. Bot. 188, 1–10. https://doi.org/10.1016/j.aquabot.2023.103670.